

# Cyclic Behaviour and Modelling of a Dissipative Connector for Cross-Laminated Timber Panel Buildings

Massimo Latour\*, Gianvittorio Rizzano

<sup>1</sup> University of Salerno, Department of Civil Engineering, mlatour@unisa.it, g.rizzano@unisa.it

## Abstract

The paper here presented aims to propose an innovative type of angle to be used in substitution of the hold-down in cross-laminated timber (CLT) panel buildings. The new connection, called XL-stub, applies a concept similar to the classical ADAS (added stiffness and damping) device. In order to characterize the force-displacement response under cyclic loads of the proposed XL-stub, an experimental campaign is presented. Successively, the effectiveness of the proposed angle is proved by analysing the non-linear response under seismic loads of a single wall alternatively equipped with hold-downs or the XL-stub.

## 1. Introduction

Timber is increasingly being used as a structural material for buildings due to the significant technical advantages that it is able to provide. The adoption of engineered wood in structural systems has recently stimulated the European residential market because of its peculiarities, such as the ease of erection at the construction site, high fire resistance, high weight/strength ratio and the possibility of combining structural layouts in energy efficient solutions. Wooden structures are well accepted in practice because they are also recognized by producers and building owners as environmentally sustainable. In fact, they rely on renewable resources and they need a manufacturing process which uses much less energy than classical structural materials, such as steel or concrete. In addition, timber buildings are able to consume carbon dioxide during their lives leading, in general, to an ecological construction process (Anink, et al., 1996; Gustavsson & Sathre, 2006; Gerilla, et al., 2007). Traditionally, most timber houses worldwide have been built with the so-called framing system, in which the bearing walls are constituted by the assemblage of columns and girders on which is fixed a plywood panel connected by means of nails or screws. In more recent times, as an alternative to the classical framing, several modern timber construction systems have been developed and applied throughout Europe with the CLT system, especially to the case of low-to-medium rise buildings where it has found its natural application.

The CLT system was initially developed in Switzerland in the early 1990s. Successively, following the green building movement, the system started its speedy growth in the early 2000s. CLT buildings gather almost all the intrinsic features of wood and, as demonstrated by past research, if properly detailed they can also provide high resistance to seismic loads. All such advantages have contributed to the spread of wooden structural systems in the countries of Europe, such as Italy, where the market has traditionally been oriented towards solutions with a monolithic structure, adopting materials such as reinforced concrete or masonry. The recent application of timber structures in high seismic regions has raised the issues related both to the evaluation of the seismic performance of timber buildings and to the update of national and European building codes, which were traditionally conceived for the design of wooden elements devoted to carrying dead and wind loads, rather than seismic loads (CEN, 2003). From the seismic standpoint, a timber panel building is conceptually similar to a box structure in which walls and floors are rigid in their planes. The structure is constituted by the assemblage of pre-cast flat cross-laminated panels used for realizing both the vertical resistant system and slabs. Such panels are manufactured by overlapping several layers of spruce planks, each layer glued orthogonally to another. The result is a massive dimension-stable stiff panel that can be easily used to erect multi-storey buildings, with excellent acoustic, thermal and fire-resistant properties. In the cross-laminated system, vertical panels are connected to each other and to the slabs by means of screws, nails and angle brackets. As long as the panels behave as rigid elements, the dissipation capacity of the whole structure subject to a seismic event is usually lumped in the connections. There are three typical

connections in CLT buildings: there is a panel–panel connection realized by overlapping a nailed or screwed strip of wood onto two subsequent pre-cast panels; a connection realized with a short angle bracket that is used to prevent horizontal slip of the panel; and a connection with a long angle used to prevent the rocking of the panel.

Recently, much experimental effort has been dedicated to this structural system in many countries, but particularly in Italy, Slovenia and Canada. In Italy, an extensive research project, the so-called SOFIE project, supported by the Trento Province and coordinated by the IVALSA-CNR Institute, has been carried out. The research work has been planned in order to validate the structural system and to investigate topics such as the seismic capacity and the fire resistance of buildings made of cross-laminated panels. In fact, the SOFIE project has included several tests on the typical connections (i.e. angles, hold-downs and panel–panel joints), tests on walls with different layouts of connections and openings, the pseudo-dynamic test of a full-scale one-storey building, full-scale shaking table tests on three-storey and seven-storey residential buildings and fire-tests on the same three-storey building tested on the shaking table (Ceccotti , et al., 2007; Ceccotti A, et al., 2006; Ceccotti, et al., 2000). The other most important experimental programme dealing with the characterization of the behaviour of cross-laminated massive panels was carried out at the University of Ljubljana in Slovenia (Dujic, 2001; Dujic & Zarnic, 2002) and at the FPInnovation Forintek in Vancouver, Canada (Popovski, et al., 2010). In the two programmes a number of experimental tests on single walls and a system of walls with different combinations of openings, boundary conditions and connections were carried out. In the work carried out by (Dujic, 2001) particular attention was paid to the analysis of the influence of the typology of the fasteners on the dissipative behaviour of the joints and to the influence of the foundations on the wall stiffness.

Despite the significant advances made in research in the last ten years, the potentialities of the CLT system still do not appear to have been fully exploited. In fact, there is a lack of knowledge regarding the actual structural behaviour of the system under seismic loads and more efforts from the scientific community are still needed in order to codify the detailing rules for buildings. Currently, Eurocode 5 (CEN, 2003) does not contain specific guidance on fabrication, design and procedures of inspection and maintenance. Furthermore, there are no satisfactory rules for designing steel joints subjected to seismic loads and the value of the behaviour factors proposed by the code are not specifically devoted to the design of timber panel buildings.

In order to provide some indications of the behaviour factor of CLT buildings, (Ceccotti , et al., 2007) carried out a set of incremental dynamic analyses by creating a numerical model of the three-storey building tested within the SOFIE project by means of the software DRAIN-3D. On the basis of these analyses, the value of the q-factor proposed by the authors for the house employing classical fastening details is equal to three. Even though the value found in (Ceccotti , et al., 2007) refers to a single case study, it demonstrates the limited dissipative capacity of timber panel buildings compared to other traditional structural systems for which typical values of the behaviour factor are much higher. The reasons for such a result can be found in the response, under cyclic loads, of the elements mainly devoted to energy dissipation, namely the hold-downs. In fact, as already demonstrated in the technical literature (Ceccotti A, et al., 2006; Gavric, et al., 2011; Dujic, 2001), hold-downs subjected to cyclic reversals even though possessing good ductility, typically exhibit a response characterized by significant pinching phenomena and, therefore, by a low capacity to dissipate energy. Within this framework, in this paper, in order to overcome the limitations provided by the adoption of the classical hold-down, the authors introduce a new type of dissipative angle, called “XL-stub”, to be applied in substitution of the classical hold-downs. It is worth noting that approaches introducing dissipative angles to beam-to-column joints of concrete and engineered timber structures have already been recently proposed by Dolce et al., (2006) and Smith et al., (2012). In particular, in order to increase the hysteretic energy dissipation of the joint, the authors have suggested the insertion at the top and bottom level of the beam of two alternative angle details: one with a zone of the flange with a reduced thickness and the other one characterized by a zone of the flange plate with a reduced thickness and circular holes.

In the following paragraphs, the concept of the new type of connector will be introduced and the results of an experimental campaign carried out at the Laboratory of Materials and Structures of the University of Salerno will be presented. In particular, the experimental analysis deals with the monotonic and cyclic testing of the innovative type of damper, which has been designed in order to

have the same stiffness and resistance as the hold-down tested in the SOFIE project. The design process has been carried out with the support of a finite element model carried out in ABAQUS 6.11 software (Simulia, 2012). Successively, the test results are used to calibrate a numerical model in the software Seismostruct (Seismosoft, 2007) with the aim of comparing the cyclic behaviour of a single wall, alternatively equipped with the XL-stub and with the classical hold-down. The obtained results show good agreement between the models and the experimental results, and significant improvement in the cyclic behaviour of cross-laminated wooden panels equipped with the innovative type of connection. The results presented are encouraging with regard to the possibility of increasing the dissipative capacity and, therefore, the behaviour factor of CLT buildings by adopting connections specifically designed for dissipating the seismic input energy.

## 2. Cyclic Behaviour of Typical Connections

It is well known that wooden cross-laminated panels exhibit brittle behaviour, which is characterized by low capacity for energy dissipation. It is for this reason that the design philosophy of timber panel buildings provides for the concentration of plasticization in the connections rather than in the wood according to a hierarchy criterion of strong-wall-weak-joint. Under this design assumption it is easy to understand that the knowledge of the behaviour of connections is of paramount importance for determining the response of the whole building under seismic loads. In fact, under severe earthquakes, the only sources of energy dissipation of a CLT building are the steel parts, that is, the angles, the nails and the screws.

CLT buildings are usually constituted by the assembly of panels made of cross-laminated wood, connected together through specific fastening elements. The three classical systems of connections are:

- *Hold-downs*, which are put at the ends of the panels and are subjected mainly to tension loads in order to prevent the uplift of the walls from the foundations or floors;
- *Angle brackets*, which are put in the middle of the panels and are mainly subjected to shear loads in order to prevent the sliding of the walls;
- *Screwed or nailed panel–panel joints*, which prevent relative movement between the panels of the walls.

In general, the ductility and hysteresis of the steel joints are mainly governed by the dissipative characteristics of the element which first undergoes plastic deformation. In the case of an angle, such an element could be the fastener (nail, screw, etc.) or the steel angle. As demonstrated by previous experimental works, the typical behaviour of traditional joints employed in CLT buildings is characterized by strong-plate-weak-connector behaviour and, therefore, the dissipative response is governed by the bearing of nails or screws into the wood. In order to show the main features of the typical hysteresis loops of classical joints, in the following, reference is made to the tension and shear tests of the connections employed in the three-storey building of the SOFIE project. The tests considered in this paper were carried out by (Gavric, et al., 2011) after the first phase of the SOFIE project. In (Gavric, et al., 2011) work, several quasi-static monotonic and cyclic tests were carried out on the hold-down WHT540 with 12 annular ringed nails 4x60 mm, whose geometry and thickness are very similar to those of the hold-down HTT22 originally used in the SOFIE project. Furthermore, also some tests both in tension and shear on the angle bracket BMF 90x116x48x3 mm with 11 annular ringed nails 4x60 mm were carried out.

The cyclic tests demonstrate that all connections, both loaded in shear and tension, are affected by significant pinching phenomena (Fig. 2). In particular, the hold-down in tension exhibits good ductility (about 25.4 mm), but a quite limited energy dissipation capacity. This is mainly due to the dissipative mechanism. In fact, the hold-down, which is designed according to a weak-connector-strong-angle philosophy, dissipates through the bearing mechanism of the nails that, at any load reversal, have to slide into the hole before restoring the force. Therefore, this failure mechanism results in significant stiffness degradation which gives rise to very narrow hysteresis loops. A similar behaviour is exhibited also by the angle bracket in tension, which mainly dissipates due to the punching of the bolt into the steel around the hole. A better behaviour is shown by the hold-down and by the angles in shear but, as

well as in the other cases, the hysteresis loops are characterized by significant pinching, limited dissipation capacity and good ductility supply (about 30 mm). In these cases, the failure mode of the hold-down in shear is typically characterized by the plasticization of the steel in the region close to the first row of nails. Conversely, the angle brackets in shear usually fail due to the contemporary yielding of the nails and failure of the wood. What is important to observe is that, since plasticization under cyclic reversals is concentrated in the connections, the hysteresis cycles of a wall subjected to cyclic loads is also characterized by a behaviour with good ductility but is affected by pinching, stiffness degradation and limited capacity of energy dissipation. This result is clearly shown in all past experiments by different researchers (Ceccotti, et al., 2000; Dujic, 2001).

The scope of the work herein presented is to propose an approach to improve the dissipative capacities of CLT buildings by enhancing the behaviour of the structural fuses, that is, the connections. As aforesaid, the typical angles employed in CLT buildings appear to possess a limited capacity of energy dissipation due to the dissipative mechanism that is imposed in the design philosophy of the angle, that is, the failure of the fasteners. In this paper, the main idea of the authors is to overturn the classical philosophy used in CLT structures by switching the joint design from the weak-fastener-strong-angle to the strong-fastener-weak-angle philosophy. Similar approaches providing the introduction of dissipative fuses in wooden structures have already been proposed in past years in experimental and numerical researches carried out at the University of Canterbury in New Zealand (Palermo et al., 2005, Palermo et al., 2006, Pampanin et al, 2006), starting from the results of analogous studies already carried out on concrete structures (Hajjar et al. 2013). In the cited works, several types of self-centering wooden beam-to-column, column-to-foundation and wall-to-foundation details combining un-bonded post-tensioned steel tendons together with dissipative hysteretic metallic dampers have been suggested. As demonstrated by Smith et al. (2008), with this technology, due to the typical “flag shaped” hysteretic loop of the dissipative zones, the damage to structural members is reduced and a fully re-centering capacity is obtained. It is worth noting that the damper proposed in this paper, if properly designed, could be effectively applied also in such a kind of rocking systems.

Therefore, in the following, the concept of the proposed angle is first shown and after an experimental analysis devoted to comparing the monotonic and cyclic behaviour of the classical and of the innovative joint will be described. Finally, the results of the experimental analysis will be used to calibrate a numerical model of the cross-laminated wall tested by (Gavric, et al., 2011) with the aim of comparing the cyclic behaviour of the same wall alternatively equipped with the classical hold-down and with the proposed XL-stub.

### **3. Concept of the Proposed Angle and Setup of the Experimental Program**

In order to better understand the principle on which the shape of the developed innovative angle is based, it is first necessary to consider the actions arising and the possible failure mechanisms occurring in a generic steel angle fixed to a wooden panel under tension loadings. As already stated, the classical hold-down has the shape of an angle with a very long stem and a short and stiffened flange plate. The stem is used to connect the angle to the wooden panel with the number of fasteners determined according to the design forces. Conversely, the flange plate is connected by means of an anchor bolt to the foundation and is stiffened in order to carry the design forces without deformations. From past experimental results, it is possible to define the failure mechanisms of an angle fixed to a wooden panel: three concerning the collapse of the wood, stem or nails in the zone fastening the angle to the wood and three concerning the collapse of the flange plate. In particular, if the stem, the fasteners or the wood are designed in order to be less resistant than the flange plate, the hold-down can fail due to the bearing of the nails into the wood, to the wood splitting or to the collapse of the stem. As already demonstrated in previous works, these three failure mechanisms are non-dissipative or characterized by a limited energy dissipation capacity. Conversely, if the flange plate is less resistant than the fasteners and less resistant than the wooden part, the possible failure mechanisms are the same as those arising from T-stub theory (Faella, et al., 2000) (Fig. 3).

Within such a theory, it is known that the bending moment arising in the flange plate of an angle in the region between the stem and the anchor bolt is governed by the ratio between the axial resistance of the bolt and the bending resistance of the plate. Depending on this ratio, there are three possible failure mechanisms. In the case of a strong bolt and a weak plate, namely mechanism type-1, the bolt is able

to fully constrain the plate and the bending moment diagram is linear along the flange with the point of contra-flexure in the middle of the plate. In the case of a strong plate and a weak bolt, namely mechanism type-3, the plate completely detaches and the bolt behaves as a hinge, giving rise to a bending moment diagram with zero-value at the bolt line and a maximum in correspondence with the stem. In all the other cases, the behaviour is intermediate between the two aforesaid extreme situations and the bolt is only able to partially restrain the bending moment. It is well known that among the three mentioned failure mechanisms, the most dissipative is type-1, which is characterized by the formation of two plastic hinges in the most stressed zones of the plate, one in correspondence with the stem-plate attachment and the other in correspondence with the bolt line. Nevertheless, previous experimental research has demonstrated that also, when the failure is due to mechanism type-1, even though the angle is able to dissipate a significant amount of energy, the hysteresis cycles are characterized by significant pinching phenomena, strength and stiffness degradation. This is due to the mechanism of plasticization of the rectangular angle which concentrates the strain demand in two finite regions, requiring a very high ductility supply in small zones (Iannone, et al., 2011; Latour, et al., 2011).

A possible approach to overcome the issues related to the limited energy dissipation capacity of rectangular angles is the one proposed in (Latour & Rizzano, 2012; Latour, et al., 2011a) dealing with the application of dissipative T-stubs to beam-to-column joints of steel structures. Such an approach makes provision for the tapering of the plate in the zone in between the stem and the bolt according to the diagram of the bending moment. In fact, it is intuitive to understand that if the plate is cut, providing a width which varies accordingly with the diagram of the bending moment, it is ideally possible to obtain the contemporary plasticization of all plate sections leading to a ductility demand distributed along the whole plate. Starting from the diagram of the bending moment arising in a plate, under the assumption of a strong bolt and a weak plate, it is easy to verify that the shape which provides the simultaneous plasticization of all plate sections is an ideal X-shape (Fig. 5).

The approach proposed by (Latour & Rizzano, 2012) follows the same principle which is applied in the design of metallic hysteretic dampers working in double curvatures, such as ADAS devices (added stiffness and damping), which are elements usually adopted in combination with chevron bracing systems (Fig. 4).

Considering only the bending moment diagram, the ideal shape is double triangular but, in actual cases, the shape of the ADAS device cannot be the ideal X-shape due to the shear and axial loads arising in the plate. In fact, a proper dimension of the mid-section is needed to withstand axial and shear actions. For this reason, ADAS devices are usually characterized by the so-called “hourglass shape”, whose geometry is defined by means of an exponential function. The mathematical formulations describing the shape of ADAS devices have been empirically determined by (Tena-Colunga, 1997) starting from the results of tests carried out at the University of Berkeley by (Whittaker, et al., 1989). With reference to the notation of Figure 5, the hourglass shape is described by the following exponential function (Tena-Colunga, 1997):

$$\begin{cases} b(z) = B e^{-\alpha \cdot z} & 0 \leq z \leq m/2 \\ b(z) = s \cdot e^{\alpha(z-m/2)} & m/2 \leq z \leq m \end{cases} \quad (0)$$

$$\alpha = \frac{2}{m} \ln\left(\frac{B}{s}\right) \quad (0)$$

where  $s$  is the width of the mid-section,  $B$  is the width of the clamped section and  $m$  is the distance between the  $s$  stressed by the maximum level of bending moment.

Therefore, the proposed angle, called in the following XL-stub, is based on the same principle of the ADAS device. The main idea is to shift the dissipative zone of the hold-down from the stem zone to the flange plate. For this scope, from the design standpoint, the stem zone has to be over-strengthened by adopting a proper number of nails and by checking the resistance of stem and wood with respect to

the force needed to yield the flange plate. In addition, in order to overcome the usual problems concerning the cyclic behaviour of rectangular steel plates subjected to bending moment and to maximize the plate energy dissipation, the proposal is to give the flange plate of the angle an hourglass shape, very similar to that usually adopted in ADAS devices (Fig. 6). In the following the design process of the proposed angle is shown and an experimental program aimed at evaluating the cyclic characteristics of the XL-stub is presented. The main results of the experimental activity are reported and also compared to that of the classical hold-down system.

### 3.1 Finite Element Modelling of the Device

The main goal of the experimental work herein presented is to provide a comparison between the cyclic behaviour of the classical hold-down and the proposed XL-stub angle. In order to show the difference in terms of hysteresis loops and to carry out a meaningful comparison, it is necessary to compare elements with the same stiffness and resistance. To this end the tested XL-stub has been designed in order to have monotonic behaviour that is largely the same as that of the hold-downs tested within the SOFIE project by (Gavric, et al., 2011).

The tested specimens have been designed with the support of a finite element model carried out by means of the ABAQUS 6.11 software (Fig. 7). The model is solid and three-dimensional using the library element C3D8R, that is, an 8-node linear brick, with reduced integration and control. ABAQUS software has several first and second order elements in its libraries. The element choice has been made in order to reduce the computational effort, by adopting C3D8R elements. The choice made does not reduce the accuracy if the meshing operation is accurate and if the instability mesh control is used to prevent the so-called hourglassing problems (Kosloff & Frazie, 1978).

In addition, in order to account for the catenary actions arising at large displacements, a static non-linear analysis was carried out. The geometric non-linearity was properly accounted for to grasp the full post-elastic behaviour of the tested angles, which are characterized, at large displacements, by second-order effects. Furthermore, in the FE model, the interactions between the plates and between hole and bolt were modelled by means of a frictionless formulation and the bolt pretension effect was modelled by imposing, in a preliminary loading step, an appropriate thermal distortion.

As mentioned above, experimental analysis was planned to verify the possibility of increasing the energy dissipation capacity under cyclic loads of the XL-stubs with respect to the classical hold-down; to this end, the design process was carried out by applying a trial and error procedure by imposing the following design conditions:

- the initial stiffness of the XL-stub is equal to that of the corresponding T-stub with rectangular flange;
- the inelastic branch of the  $F-\delta$  curve of the XL-stub fits that of the hold-down tested within the SOFIE project by (Gavric, et al., 2011).

In order to achieve the design goals, within the design process, the following three geometrical parameters were considered: the distance  $m$  between the bolt and the plastic hinge, the width of the plate  $B$ , and the thickness of the plate  $t$ . The three parameters were chosen as the main design parameters because they strongly affect the angle's overall behaviour and, in particular, initial stiffness, resistance and the ductility. In fact, as reported in (Latour & Rizzano, 2012), where a mechanical model able to predict stiffness, resistance and ductility of X-shaped T-stub has been developed, the initial stiffness is related to the ratio  $(Bt^3/m^3)$ , the plastic resistance corresponding to the knee of the force-displacement curve of the T-stub depends mainly on the parameter  $(Bt^2/m)$  and the ductility is governed by the parameter  $(m^2/t)$ . It is clear that the reduction of the section width along the plate due to the hourglass shape leads mainly to a reduction in the angle stiffness which can be recovered by increasing the width  $B$  and the thickness  $t$  and by reducing the distance  $m$ . The simultaneous respect of the previous design conditions provided the most appropriate combination of values of the three geometrical design parameters. The trial and error procedure performed for designing the above geometrical parameters of the XL-stub has been based on the preliminary prediction of the stiffness, strength and ductility provided by the mechanical model described in detail

in (Latour & Rizzano, 2012). For the sake of clarity the equations used in the design process are here reported:

### **Stiffness**

$$K_{0,HS} = \zeta \frac{EBt^3}{m^3} \quad (3)$$

where:

$$\begin{cases} \zeta = \frac{2(B-s)}{3B} \frac{4(B-s)^2}{4(B-s)A_1 + 4(B-s)A_2 - 2A_3} \\ A_1 = [(B-s) + (B-2s)\ln(B/s)] \\ A_2 = [(s-B) + B\ln(B/s)] \\ A_3 = [(3s-B)(B-s) + 2B(B-2s)\ln(B/s)] \end{cases} \quad (4)$$

and  $t$  is the thickness of the flange plate.

### **Yield Resistance**

$$F_y = \frac{4M_y}{m} = \frac{2}{3} \cdot \frac{B_{eff} t^2 f_y}{m} \quad (5)$$

where:

$$B_{eff} = \frac{\alpha B m}{2} e^{\left(1 - \frac{\alpha m}{2}\right)} \quad (6)$$

and  $f_y$  is the material yield stress.

### **Ductility supply**

$$\delta_u = \frac{\varepsilon_u m^2}{t} \quad \delta_y \leq \delta \leq \delta_u \quad (7)$$

where  $\varepsilon_u$  is the material ultimate strain.

As a result of the design process in Figure 8, the comparison between the force-displacement response of the XL-stub predicted by the finite element model and that of the hold-down tested in (Gavric, et al., 2011) is reported. It is possible to note the good agreement between the force-displacement curve of the dissipative angle and that of the hold-down. Furthermore, from the finite element model it is possible to appreciate the distribution of the stresses within the plate and the distribution of the plasticization that involve the whole plate section, confirming the spread of plasticization within the whole flange plate (Fig. 9).

## **3.2 Experimental Setup**

In order to compare the monotonic and cyclic behaviour of the classical hold-down and the proposed angle, an experimental program was set up. All the tests were carried out at the Laboratory of Materials and Structures of the University of Salerno by means of a universal testing machine Schenck Hydropuls S56 (maximum load 630 kN, piston stroke +/- 125 mm). The campaign included one uniaxial monotonic test (A05-M), three cyclic tests at constant amplitude (A01-C15, A02-C25, A03-C30) and one cyclic test at variable amplitude (A04-CV) (Table 2). The scope of the constant amplitude cyclic tests is to define the fatigue-life curve of the angle that is a fundamental tool in defining the damage and the collapse condition of the XL-stub in cyclic and dynamic analyses. The variable amplitude test was carried out in order to verify the hypothesis of linear accumulation of damage, as proposed by (Miner, 1945). Furthermore, the cyclic tests were carried out in order to

compare the dissipative capacities of the XL-stubs with respect to the hold-downs.

The tested specimens consisted of a panel of larch with dimension 518x255x72 mm on the top of which was fixed a very stiff and strong T-stub and on the bottom a couple of the designed XL-stubs (Fig. 10). The elements were fastened through eight 8.8 class M12 bolts. The steel grade of the angles was S275 (CEN, 2005). The connection of the angles to the wood was designed following the rules provided by Eurocode 5 in order to have fastener over-strength with respect to the load carried by the tapered flange plate. In this way, the bearing failure is avoided and the failure of the dissipative zone is promoted. The identity tag of the specimens allows identifying all the examined cases. After the symbol A, which stands for angle, there is an index that individuates the progressive number of the tests. Symbols –M, –C and –CV individuate the monotonic, cyclic with constant amplitude and cyclic with variable amplitude tests. Finally, the last number defines the amplitude of the cycles (in *mm*) in the case of the constant amplitude tests.

All tests were quasi-static and, in particular, they were conducted under displacement control, with a variable speed from 0.3 mm/s to 0.6 mm/s for the cyclic tests with constant amplitude (0.01 Hz), from 0.5 mm/s to 0.9 mm/s for the cyclic test at variable amplitude and with a constant speed of 0.025 mm/s for the monotonic test. In addition, coupon tensile tests were performed in order to establish the mechanical properties of the base material constituting the plates. The values of the mechanical properties are given in Figure 11 and in Table 3.

#### **4. Experimental Analyses of Dissipative Devices**

All tests were executed using the same specimen. At the end of each test, the only parts that were substituted were the couple of angles that are the elements which undergo damage. In the following, the results obtained from the cyclic and monotonic tests are reported, showing the significant improvement of the behaviour of the traditional detail.

##### **4.1 Monotonic Test Results**

The monotonic test (A05-M) was carried out under displacement control at a constant speed of 0.025 mm/s. The test was stopped because the piston stroke of the universal machine was reached. Nevertheless, the ultimate displacement obtained during the test was very high and no damage or cracks were evidenced. As predicted by the FE modelling, the experimental results of the monotonic tests were very close to the one provided by hold-down tested by (Gavric, et al., 2011). In fact, the monotonic force-displacement curve has a behaviour which is very similar in terms of force and stiffness to the cyclic envelope of the test on the hold-down of the SOFIE project, but with higher ductility that is almost two times greater (Fig. 13).

As desired in the design phase, all the deformation capacity of the specimen was concentrated in the flange plate of the XL-stub. No wooden or steel part evidenced damage, but significant second-order effects were shown. This can be clearly noted also from the force-displacement curve of the angle. In fact, in the plastic range, after a first phase of strain-hardening which follows the complete yielding of the plate, there is a slight increase in the stiffness which is due to the catenary effects that arise in the plate. These second-order effects are demonstrated by the plasticization of the stem of the angle in the zone in between the attachment with the flange plate and the first row of bolts (Fig. 12). In this zone the stem works as a cantilever beam fully constrained in the bolts. It is interesting to note that the significance of this effect depends on the geometry of the stem that governs the post-elastic stiffness at high displacements.

##### **4.2 Cyclic Test Results**

###### *Constant Amplitude Tests (A01-C15, A02-C25, A03-C30)*

As already underlined, the experimental analysis was planned in order to verify the possibility of increasing the energy dissipation capacity under cyclic loads of classical hold-downs by overturning the classical design philosophy from the nail to the flange plate plasticization. The purpose of the study is comparative. In fact, the basic idea is to show that a dissipative hold-down can be properly

designed in order to have a monotonic behaviour very close to that of a classical hold-down but a more dissipative behaviour under cyclic loads.

To this end, a series of cyclic tests on the XL-stubs, specifically designed for dissipating energy, was planned. In particular, as aforesaid, three constant amplitude tests were performed with the aim of defining the cyclic behaviour and the fatigue-life curve of the element. The fatigue-life curve is a powerful tool for carrying out incremental dynamic analysis in order to define the damage and the collapse condition of an element.

The displacement amplitudes of the tests, equal to 15, 25 and 30 mm, were chosen aiming to cover a range of displacements that is compatible with the typical structural applications of timber panel buildings (Ceccotti, et al., 2000). In fact, considering the results of the SOFIE project, under the most severe seismic events considered, the uplift of the hold-down is equal to 25 mm. All the cyclic tests showed the same collapse mechanism for all the XL-stubs. In particular, after a certain number of cycles, the formation of a crack in correspondence with the flange plate-stem connection was evidenced. It is clear that the failure of the XL-stub occurs in that zone, even though the angle is ideally designed to have the same resistance in all the plate sections, because it is the least resistant region of the plate due to the welding process. This is the reason why the cracking of the flange plate first developed at the welds and progressively propagated through the plate leading to the complete fracture after a high number of cycles (Fig. 14). Under cyclic loads, such behaviour gave rise to a progressive deterioration up to the failure of stiffness, resistance and energy dissipation capacity. The expected spread of plasticization within the whole flange of the angle is confirmed by the shots taken by means of an FLIR thermal camera in the first cycles of loading. The measurement of the heat along the flange during the first six cycles confirms a uniform thermal state and, therefore, a spread of the plasticization also in the middle regions of the plate (Fig. 15).

In terms of hysteretic behaviour (Fig. 16), the design goal of the angle appears to have been achieved. In fact, the cyclic behaviour in all the three constant amplitude tests is characterized by a very stable response with low rates of stiffness, strength and energy dissipation capacity degradation before the quick failure due to the development of the crack in the plate. It is evident that the hysteretic response of the developed XL-stub is almost unaffected by pinching phenomena which usually characterize the behaviour of the failing in the nails of the classical hold-downs due to bearing. This result is due to the particular shape provided by the flange which leads to a very high dissipative capacity under cyclic loadings. The results here reported are represented in the following also in terms of fatigue-life curve.

#### *Variable Amplitude Test (A04-CV)*

The test at variable amplitude as carried out in order to verify the validity of the linear accumulation of damage rule proposed by Miner. The loading protocol followed is inspired by that developed in (AISC, 2005) for tests on steel connection details. Within this protocol, the amplitude of the cycles progressively increases up to collapse, by following the scheme reported in Table 4, in which the velocity, the number and the amplitude of the cycles is also reported.

In this case, the test results also evidence a satisfactory hysteretic response of the angle under cyclic loads with a large amount of dissipated energy. In fact, the response has been characterized by wide and stable cycles with almost no degradation phenomena up to failure, as in cases of tests at constant amplitude. The failure arose after the 42<sup>nd</sup> cycle at an amplitude of 41.5 mm. In particular, the collapse of the specimen occurred due to the contemporary fracture of the plate in correspondence to the weld and of the bolt line. This result testifies again the efficiency of the design criteria of the element, which is able to dissipate the external energy by means of the plastic engagement of the whole plate.

From the analysis of the response under variable amplitude cycles, it is evident that the angle is able to dissipate an amount of energy that is much greater compared to that of the classical hold-down. In fact, in comparison to the hold-down tested in (Gavric, et al., 2011), it is possible to observe that, even though the XL-stub has been subjected to a displacement history much more demanding compared to the loading history adopted in the SOFIE project, the cyclic response has been much more stable and dissipative, and also with higher ductility. All these results are better demonstrated in the following paragraph dealing with the characterization of fatigue life and comparing the behaviour of the classical detail with respect to the innovative.

### 4.3 Fatigue Life

Aiming to provide a synthetic representation of the cyclic behaviour of the XL-stub, starting from the results of the cyclic tests, the fatigue-life curve was defined. To this end, it is first necessary to define the conventional collapse criteria. Usually, the definition of the conventional collapse is not trivial and, in fact, a universally recognized approach does not exist. According to previous scientific works, it is known that the collapse condition of an element subjected to cyclic loads can be individuated in correspondence with a prescribed value of the stiffness, strength or energy dissipation capacity degradation. Within the present work, the collapse condition is defined by checking the degradation of the energy dissipation capacity, because in this way it is possible to account for the overall behaviour of the XL-stub, including also the influence of the reduction of stiffness and strength. According to (Castiglioni & Calado, 1996) the collapse of a specimen can be defined when the maximum degradation of the energy dissipation capacity achieves a value equal to 50% of the energy dissipated in the first loading cycle. In fact, as stated by (Castiglioni & Calado, 1996), usually after a degradation of about 50% a sudden reduction of the energy dissipation capacity occurs, leading to the quick failure of the considered element.

In accordance with this criterion, the individuation of the number of cycles at failure for the constant amplitude tests was carried out. In particular, Figure 19 depicts the number of cycles in the tests before collapse was reported. The maximum value of the degradation of the energy dissipation capacity was achieved for the three tests at the amplitudes of 15, 25 and 30 mm after 107, 43 and 29 cycles respectively.

Therefore, starting from the knowledge of the number of cycles at collapse, it is possible to obtain the fatigue-life curve that defines the relationship between the number of cycles needed to attain the collapse condition and the displacement amplitude. It is well known that in the low-cycle range the fatigue curves can be represented by means of straight lines in bi-logarithmic scales. In particular, the number of plastic reversals at failure  $n_c$  can be related to the total displacement amplitude  $\delta$  by means of the following relationship (Miner, 1945):

$$\delta = an_c^b \quad (8)$$

where  $a$  and  $b$  are two regression parameters to be found experimentally. Starting from the results of the cyclic tests, the fatigue-life curve depicted in Figure 20 was defined, obtaining a value of the slope  $b$  equal to -0.53 and an intercept with the vertical axis  $a$  equal to 177.8. It is useful to note that the value of the slope found in this work is in agreement with that found in previous experiments carried out by several authors (Faella, et al., 1998; Castiglioni & Calado, 1996; Latour & Rizzano, 2012).

As already stated, the fatigue-life curve is one of the most powerful tools to describe the damage state of an element. In fact, through the fatigue-life curve, under the assumption of linear accumulation of damage, it is possible to define the accumulated deterioration of an element under a generic loading history, starting from the knowledge of the degradation expected at each amplitude value. In fact, according to Miner's rule the total damage can be expressed as:

$$D = \sum_{i=1}^{n_c} \frac{n_i}{n_c} \quad (9)$$

where  $n_i$  is the number of cycles at a certain value of the displacement amplitude and  $n_c$  is the number of cycles at failure that the element can withstand at that amplitude value.

In order to evaluate the accuracy of the obtained fatigue-life curve in predicting the collapse of the XL-stub, Miner's rule has been applied to test A04-CV in order to predict the failure cycle. To this end, for each one of the amplitudes given in Table 4 the number of cycles at collapse has been evaluated by means of Equation 8:

$$n_c = \left( \frac{\delta}{a} \right)^{-1/b} \quad (10)$$

and the accumulated damage at the  $i$ -th cycle has been evaluated by means of Equation 9, leading to the result depicted in Figure 21. The reported result leads to a prediction of the failure after 43 loading cycles, which is almost the same value found in the experimental test. In fact, as said in the previous paragraph, the failure of the XL-stub tested under variable cyclic amplitude occurred at the 42<sup>nd</sup> cycle. This result confirms the accuracy of the hypothesis of linear accumulation of the damage and confirms that the obtained fatigue-life curve is able to predict the failure of the XL-stub.

#### 4.4 Energy Comparisons

In order to better demonstrate the potentialities of the developed system, a direct comparison with the hold-down tested within the SOFIE project was undertaken. In Figure 22 the hysteretic curves of the two details are overlapped in order to grasp the difference in terms of energy dissipation capacity of the XL-stub in comparison with the hold-down.

In particular, it is easy to note how the different types of hysteresis of the two elements affect the cyclic response. The hold-down is characterized by significant pinching due to its dissipative mechanism that relies mainly on the plasticization of the nails due to bearing. In fact, as already said, at the reversals the nails have to slip into the deformed holes before restoring the force. It is for this reason that after unloading, the re-loading of the hysteretic curve is characterized by a first branch that is almost horizontal due to the nail slippage and a second branch with a significant increase in stiffness and energy dissipation (Fig. 22).

On the contrary, the XL-stub shows a behaviour that is much more dissipative due to the shift in the mechanism of plasticization from the stem to the plate. In addition, the particular hourglass shape of the plate provides a high dissipative capacity that is demonstrated by the comparison of the amount of energy dissipated at collapse.

Such a difference can be easily evidenced by comparing single cycles at different values of the amplitude. In Figure 23, the comparison of the hysteresis loops at displacements of 9, 20, 35 mm is reported. From this comparison, an improvement in the energy dissipation capacity results that varies in the range from 36% to 128% depending on the displacement amplitude value. It is worth noting that the difference is more significant with respect to the amplitude increase (Table 5). This result is again due to the failure mechanism of the classical hold-down. In fact, as long as the amplitude of the cycle is greater, pinching phenomena become more significant due to the progressive oval shaping of the wooden holes.

Finally, in Figure 24, the comparison in terms of dissipated energy between the hold-down and the XL-stub is reported. The difference in energy dissipation of the two elements is significant. In fact, the XL-stub at collapse dissipates almost 30 times the energy dissipated by the hold-down of the SOFIE project. This result appears very encouraging with regard to the possibility of improving the dissipative behaviour of CLT buildings by enhancing the energy dissipation capacity of the structural fuses. Therefore, in the following paragraph, the first comparison in a case study is carried out.

### 5. Numerical Modelling of a Single Wall

In order to carry out a more complete comparison between the behaviour of the hold-down and that of the proposed innovative angle, a numerical model able to simulate the response of a single wall was undertaken by means of the software SeismoStruct. In particular, the main goal of the work presented in this section is to compare the dissipative capacities of a CLT wall alternatively equipped with the hold-down and with the XL-stub.

To this end, starting from the experimental results presented in the previous section together with those obtained by (Gavric, et al., 2011), the hysteretic curves of the connectors, that is, the angles and hold-down or XL-stub, have been mathematically modelled by means of non-linear springs, defined according to the multi-linear model of (Sivaselvan & Reinhorn, 1999). Successively, an FE model of

one of the walls tested within the SOFIE project was set up in order to define two cases: the first with the classical hold-downs and the second with the XL-stubs.

The wall considered in this paper is the one tested in the SOFIE project within the first part of the activity, preparatory to the shaking table test, on the three-storey building. It is a full-scale test on a single wall with dimensions 295x295 cm anchored to a stiff floor with two hold-downs at the ends and four angle brackets in the middle. The hold-downs are located at a distance of 50 mm from the end of the wall and the angle brackets are put at a spacing of 450 mm according to the scheme reported in Figure 25.

The connectors employed in this test are the same as those reported previously and whose hysteretic response is given in Figure 2 (Gavric, et al., 2011). The numerical model has been defined under the hypothesis of strong wall and weak connectors by considering that all the deformability is concentrated only in the connecting elements. Therefore, the developed model is constituted by a rigid frame realized by the assemblage of infinitely rigid struts connected to the floor by means of non-linear springs representing the angle brackets and the hold-downs or the XL-stubs. The shear and tensile behaviours of the non-linear springs have been modelled by means of the cyclic law proposed by (Sivaselvan & Reinhorn, 1999) that is able to account for the stiffness, strength and energy dissipation capacity degradation that characterize the cyclic response of the considered elements. In particular, the hysteretic cyclic law proposed by (Sivaselvan & Reinhorn, 1999) is defined by 15 parameters. Some of these parameters, such as the stiffness or the yield force, have been defined directly from the experimental curves, while the degradation parameters, being HC, HDB, HBE and HS of Table 6, have been calibrated by minimizing the difference in terms of energy dissipated by the experimental tests and the mathematical model. To this end, a user sub-routine implementing the mathematical model of (Sivaselvan & Reinhorn, 1999) has been set up in Visual Basic for Application in order to minimize the energetic error by checking the coefficient of determination  $R^2$ :

$$R^2 = \sum_{i=1}^n \frac{(\hat{y}_i - y^*)^2}{(y_i - y^*)^2} \quad (6)$$

where  $\hat{y}_i$  is the simulated value,  $y^*$  is the mean value of the experimental data and  $y_i$  are the experimental values.

The results of the numerical calibrations of the single connectors are reported in Figure 26, showing the obtained accuracy in predicting the energy dissipated and the approximation in predicting the cyclic response of all the considered elements in terms of force-displacement behaviour. It is important to remark that, in order to simulate the unilateral constraint of the foundation in compression the non-linear springs representing the behaviour of the angles, hold-downs and XL-stubs have been put in parallel with a gap spring characterized by an infinite stiffness in compression and a very low stiffness in tension.

The model assembled in Seismostruct is reported in Figure 27 showing the hypothesized scheme. The wall is modelled with six rigid struts and the load is applied under displacement control at the top end of the panel. The analysis has been carried out by imposing the same loading history as defined in the experimental test and by carrying out a static non-linear time-history analysis. In particular, the loading history is characterized by a cyclic displacement increasing up to the value of 56 mm. In order to establish the failure of the wall, the angles and hold-downs were monitored. In particular, dealing with the hold-down and with the angle brackets, according to the criteria proposed by (Ceccotti, et al., 2007) the collapse has been defined in correspondence with the ultimate displacement deriving from the cyclic loading histories reported in Figure 2. Conversely, in the case of the XL-stub, a more accurate criterion is considered by evaluating the progressive damage of the element by means of the fatigue-life curve previously defined (Fig. 20). The accumulated damage is estimated according to Miner's rule, by following the procedure previously shown.

## 5.1 Results

In this section the results obtained by the two models of the wall, one with the hold-down and the other with the XL-stub, are presented. The former is necessary to evaluate the accuracy of the finite element model carried out in the SeismoStruct software in predicting the response of the wall tested by (Gavric, et al., 2011). Conversely, the latter model is necessary to evaluate the improvement of the hysteretic response of the wall under the hypothesis of substitution of the hold-down with the XL-stub. In Figure 29 the comparison, in terms of panel-top-displacement base-shear, of the experimental test versus the prediction provided by Seismostruct is reported. The obtained results appear to be in good agreement with the experimental values both in terms of hysteretic behaviour and in terms of predicting the energy dissipated. Furthermore, the collapse condition, which occurs due to the failure of the hold-down in tension, is individuated with sufficient approximation in correspondence with the maximum displacement of the loading history.

The comparison in terms of energy dissipation shows good agreement between the model and the experimental test. In fact, as shown in Table 7, the model overestimates the energy, on average, by only 6% with a standard deviation of 9.4%.

The numerical model was calibrated, confirming the possibility of modelling the response of a wall starting from the mathematical modelling of the single hysteretic behaviour of the angle brackets and the hold-down. The same model was used to hypothesize the substitution of the hold-down with the XL-stubs.

The obtained improvement in terms of hysteretic behaviour and energy dissipation capacity appears significant. In fact, even though the response of the wall equipped with the XL-stub is still characterized by pinching phenomena, these effects are reduced due to the introduction of the stable hysteretic response of the XL-stub. In fact, the energy dissipation capacity with respect to the original wall is increased by about 43%. Furthermore, it is of fundamental importance to note that, at the end of the imposed loading history, the XL-stub did not fail and, in particular, according to the fatigue-life curve previously defined, has accumulated damage determined by means of Miner's rule equal to 0.1, that is, a value still quite far from the collapse condition.

Therefore, it appears that the wall equipped with the XL-stubs is characterized by a significantly higher dissipation capacity and ductility supply due to the improved behaviour of the hysteresis of the main sources of energy dissipation, namely the hold-downs. In Figure 30 the simulated force-displacement response of the hold-down and that of the XL-stub are compared, showing again the significant difference in terms of dissipative capacities of the two joint details.

Finally, in order to prove the efficiency of the proposed system, also time-history analysis of the same walls, alternatively equipped with hold-downs and XL-Stubs, have been performed. The main goal of these analysis is to compare the response of the two walls in terms of displacement demand required by a ground motion. To this scope, four simulations have been carried out considering the historical earthquakes reported in Table 8, which have been chosen among ten earthquakes previously selected in order to match the EC8 Spectrum delivered in Fig.31.

The results of the performed analysis are represented in Fig.32. They have been carried out considering a PGA leading to a peak response expressed in terms of drift of the wall equipped with the classical hold-downs contained in between 1% and 1.5%. The results of the time-history analysis reported in Fig.32 demonstrate that the two walls, one equipped with the hold-downs and the other one with the XL-Stubs, before plasticization provide approximately the same response, while, when the plastic engagement and the energy dissipation of the connectors at the base of the walls become significant, the response also becomes substantially different. In fact, the wall equipped with the XL-Stubs provides always a peak response lower than the corresponding peak response of the wall equipped with the hold-downs, due to the increased energy dissipation provided by the dissipaters. In particular, in the considered cases, the peak response in terms of drift is reduced in a percentage contained between the 30 % and the 78% depending on the considered accelerogram.

In conclusion, the developed analysis prove that the proposed system is able to provide a double benefit both on the capacity and on the demand side. In fact, on the capacity side, it has been demonstrated that the proposed angle is able to provide an improved response in terms of fatigue life, energy dissipation and displacement capacity. Conversely, on the demand side, it has been demonstrated by means of the time-history analysis that, due to the supplementary source of energy

dissipation provided by the application of the XL-Stubs, also the peak response required by the earthquake is significantly reduced.

## 6. Conclusions

In this work, an approach to improve the behaviour of CLT buildings has been presented. In particular, aiming to improve the dissipative capacities of CLT buildings, the concept of a new type of angle to be used in substitution for the classical hold-down has been introduced. Successively, the possibility of enhancing the behaviour of CLT buildings by using the proposed connector has been demonstrated by directly comparing the cyclic behaviour of the classical hold-down with respect to the proposed XL-stub. To this end, the work was organized in two phases.

In the first phase, after preparatory work in designing the proposed angle, experimental analysis was carried out at the Laboratory of Materials and Structures of the University of Salerno. Within this experimental analysis, one monotonic test, three cyclic constant amplitude tests and one cyclic test at variable amplitude were carried out on the proposed dissipative angle, designed to have the same stiffness and resistance as the classical hold-down. The results of the experimental analysis demonstrated significant improvement in the hysteretic behaviour of the classical hold-down, mainly because the proposed angle was designed to dissipate the energy in the flange plate rather than in the nails or the screws. In particular, in order to maximize the energy dissipation capacity of the angle, the flange plate was designed with a shape similar to that usually employed for ADAS devices.

In the second phase, a comparison of a single wall alternatively equipped with hold-downs or with XL-stubs was carried out by means of the software Seismostruct. In order to compare the behaviour of the wall with the two types of connectors, the hysteretic behaviour of all the considered connectors was mathematically modelled with the aim of carrying out a static non-linear analysis, simulating the experimental test on an isolated wall carried out by (Gavric, et al., 2011). In this case also, the obtained results demonstrate a significant improvement in terms of dissipative capacities and ductility supply of the wall equipped with the XL-stubs. Furthermore, at the end of the simulated tests, the hold-down collapsed due to the achievement of the ultimate displacement, while the XL-stub exhibited very limited damage that can be estimated by means of the fatigue-life curve as being equal to 10% of the maximum damage. The obtained results appear very encouraging with regard to the possibility of improving the seismic behaviour of CLT buildings by enhancing the cyclic behaviour of the structural fuses by adopting the proposed XL-stubs.

## References

- AISC, 2005. *Seismic Provisions for Structural Steel Buildings*. ed. Chicago, Illinois: .
- Anink, D., Boonstra, C. & Mak, J., 1996. *Handbook of Sustainable Building*. London: James & James.
- Castiglioni, C. & Calado, L., 1996. *Low-Cycle Fatigue Behaviour and Damage Assessment of Semi-Rigid Beam-to-Column Connections in Steel*. Istanbul,.
- Ceccotti, A., Follesa, E. & Karacabeyli, E., 2000. *3D Seismic Analysis of Multi-Storey Wood Frame Construction*. British Columbia, Canada,
- Ceccotti, A., Follesa, M. & Lauriola, M., 2007. *Quale fattore di struttura per gli edifici multipiano a struttura di legno con pannelli a strati incrociati?*. Bari, s.n.
- Ceccotti A, Follesa, M., Lauriola, M. & Sandhaas, C., 2006. *SOFIE Project - Test Results on the Lateral Resistance of Cross Laminated Wooden Panels*. Geneva,.
- CEN, 2003. *Eurocode 5: Design of Timber Structures - Part 1-1: General - Common Rules and Rules for Buildings*. s.l.
- CEN, 2005. *Eurocode 3: Design of Steel Structures - Part 1-1: General Rules and Rules for Buildings*. s.l.

- Dolce, M., Moroni, C., Nigro, D., Ponzo, F.C., Santarsiero, G., Di Croce, M., De Canio, G., Renieri, N., Campanero, M., Berardis, S., Goretti, A., Spina, D., Lamona, B., Marnetto, R. (2006). "TREMA Project: Experimental evaluation of Seismic Performance of a RC ¼ Scaled Model Upgraded with the DIS-CAM System Proceedings of the fib 2<sup>nd</sup> International Congress, Naples, Italy.
- Dujic, B., 2001. *Experimental Supported Modeling on Response of the Timber-Frames Wall Panels to Horizontal Cyclic Load*. Ljubljana, Slovenia: UL FGG.
- Dujic, B. & Zarnic, R., 2002. *Influence of Vertical Load on Lateral Resistance of Timber Framed Walls*. Kyoto, Japan,
- Faella, C., Piluso, V. & Rizzano, G., 1998. Cyclic Behaviour of Bolted Joint Components. *Journal of Constructional Steel Research*, Volume 46.
- Faella, C., Piluso, V. & Rizzano, G., 2000. *Structural Steel Semi-Rigid Connections*. Boca Raton: CRC Press.
- Gavric, I., Ceccotti, A. & Fragiaco, M., 2011. *Experimental Cyclic Tests on Cross-Laminated Timber Panels and Typical Connections*. Bari,
- Gerilla, G., Teknomo, K. & Hokao, K., 2007. An Environmental Assessment of Wood and Steel Reinforced Concrete Housing Construction. *Building and Environment*, 42(7), pp. 2778–2784.
- Gustavsson, L. & Sathre, R., 2006. Variability in Energy and Carbon Dioxide Balances of Wood and Concrete Building Materials. *Building and Environment*, 41(7), pp. 940–951.
- Hajjar, F., Sesen, A., Jampole, E., Wetherbee, A., 2013. A Synopsis of Sustainable Structural System with Rocking, Self-Centering and articulated Energy Dissipating Fuses. Report No. CEE-2013-01. Northeastern University, Boston.
- Iannone, F., Latour, M., Piluso, V. & Rizzano, G., 2011. Experimental Analysis of Bolted Steel Beam-to-Column Connections: Component Identification. *Journal of Earthquake Engineering*, 15(2), pp. 214–244.
- Kosloff, D. & Frazie, G., 1978. Treatment of Hourglass Patterns in Low Order Finite Element Codes. *International Journal for Numerical and Analytical Methods in Geomechanics*, Volume 2, pp. 57–72.
- Latour, M., Piluso, V. & Rizzano, G., 2011. Cyclic Modeling of Bolted Beam-to-Column Connections: Component Approach. *Journal of Earthquake Engineering*, 15(4), pp. 537–563.
- Latour, M., Piluso, V. & Rizzano, G., 2011a. Experimental Analysis of Innovative Dissipative Bolted Double Split Tee Beam-to-Column Connections. *Steel Construction*, June, 4(2), pp. 53–64.
- Latour, M. & Rizzano, G., 2012. Experimental Behavior and Mechanical Modeling of Dissipative T-Stub Connections. *Journal of Structural Engineering*, 138(2), pp. 170–182.
- Miner, M., 1945. Cumulative Damage in Fatigue. *ASME Journal of Applied Mechanics*, Volume 67, pp. A159–A164.
- Palermo, A., Pampanin, S., Buchanan, A., and Newcombe, M. (2005). "Seismic Design of Multi-Storey Buildings using Laminated Veneer Lumber (LVL)." *2005 NZSEE Conference*, Wairaki, New Zealand, pp. 8.
- Palermo, A., Pampanin, S., Fragiaco, M., Buchanan, A., and Deam, B. (2006). "Innovative Seismic Solutions for Multi-Storey LVL Timber Buildings." *World Conference in Timber Engineering, Portland, USA*, pp. 8.
- Pampanin, S., Palermo, A., Buchanan, A., Fragiaco, M., and Deam, B. (2006). "Code Provisions for Seismic Design of Multi-Storey Post-Tensioned Timber Buildings." *CIB W18 Workshop on Timber Structures, Florence, Italy*, pp. 12.

Popovski, M., Schneider, J. & Schweinsteiger, M., 2010. *Lateral Load Resistance of Cross-Laminated Wood Panels*. VancouverSeismosoft, 2007. *A Computer Program for Static and Dynamic Nonlinear Analysis of Framed Structures*: seismosoft.com.

Simulia, 2012. *Abaqus Manual v6.11*

Sivaselvan, M. & Reinhorn, A., 1999. *Hysteretic Models for Cyclic Behavior of Deteriorating Inelastic Structures*, Buffalo: MCEER/SUNY.

Smith, T., Pampanin, S., Buchanan, A., Fragiacomio, M. *Feasibility and Detailing of Post-tensioned Timber Buildings for Seismic Areas*. 2008. Proceedings of NZSEE 2008 Conference, Wairaki, New Zealand.

Smith, T., Ponzo, F.C., Di Cesare, A., Auletta, G., Pampanin, S., Carradine, D., Palermo, A., Nigro, D., 2012. *Seismic Performance of a Post-Tensioned Glue Laminated Beam to Column Joint: Experimental and Numerical Results 2012*. Proceedings of WCTE Conference, Auckland, New Zealand.

Tena-Colunga, A., 1997. Mathematical Modelling of the ADAS Energy Dissipation Device. *Engineering Structures*, 19(10), pp. 811–821.

Whittaker, A., Bertero, V., Alonso, J. & Thompson, C., 1989. *UCB/EERC-89/02 Earthquake Simulator Testing of Steel Plate Added Damping and Stiffness Elements*, Berkeley: College of Engineering.



**Figure 1.** Hold-down, angle bracket and screwed-joints

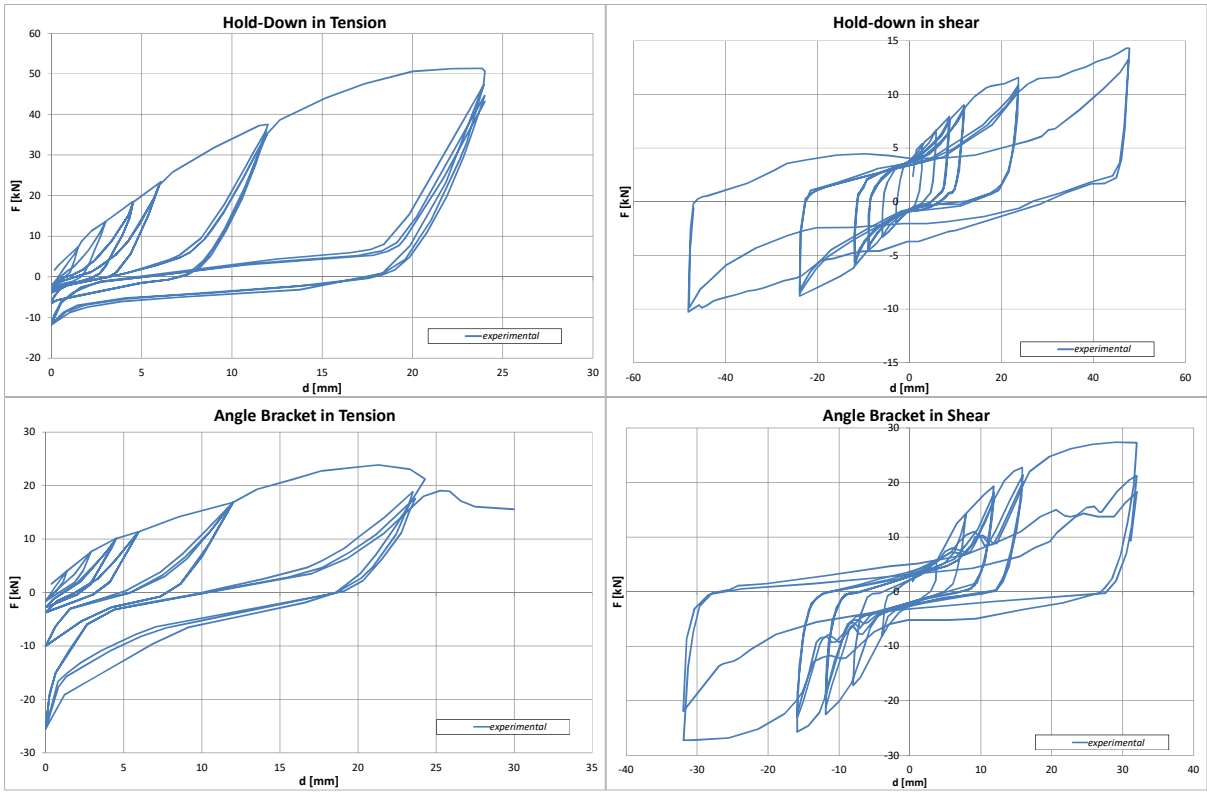


**Figure 2.** Hysteresis loops of a hold-down loaded in tension and of an angle bracket loaded in shear (Gavric, 2011)

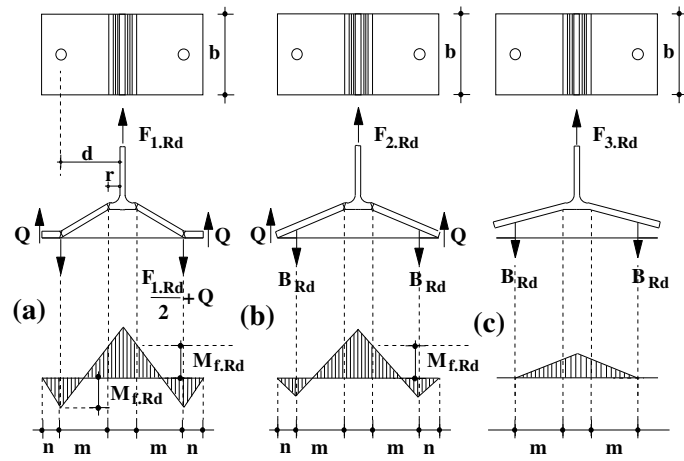


**Figure 3.** Failure modes of a bolted T-stub (Faella et al., 2000)

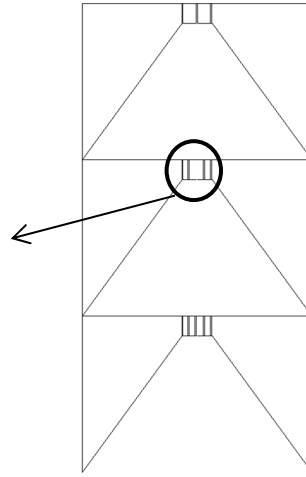
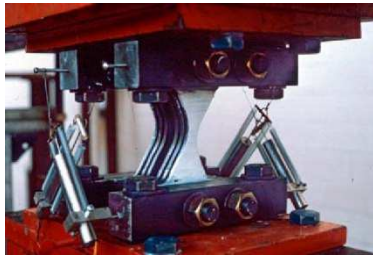


**Figure 4.** Frames with ADAS devices

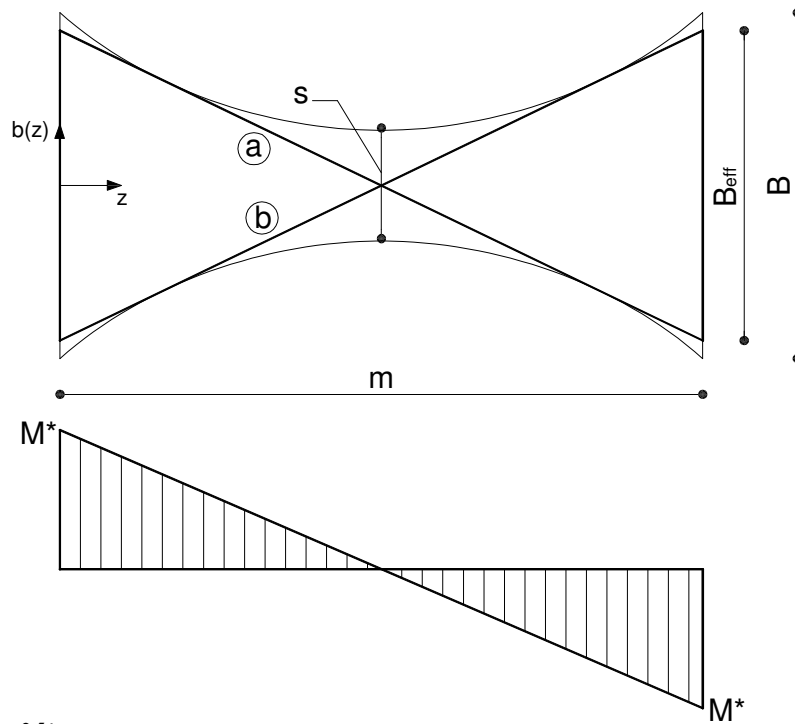
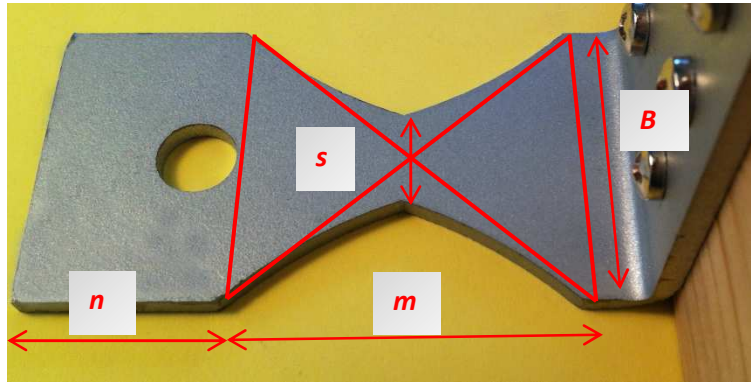


**Figure 5.** Bending moment diagram arising on the tapered flange



**Figure 18.** Failure of the XL-stub after the variable amplitude cycles test



**Figure 6.** Concept of the developed dissipative angle (study model)

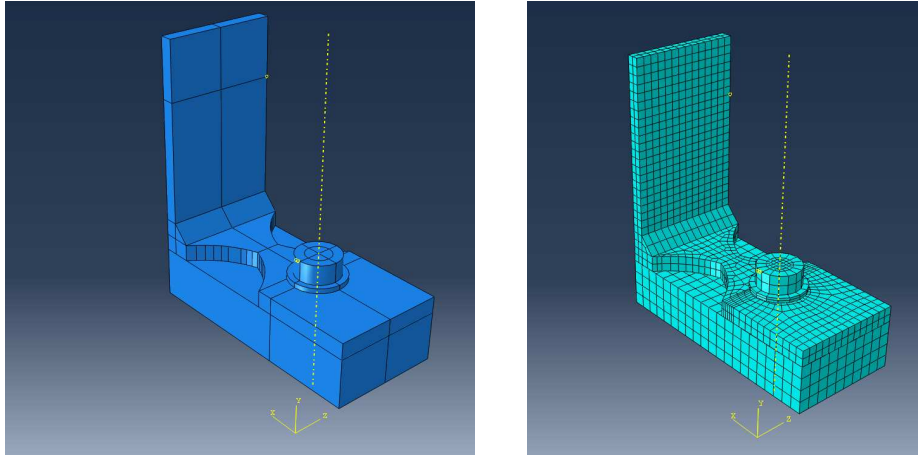


**Figure 7.** Assembly and mesh of the FE model in ABAQUS

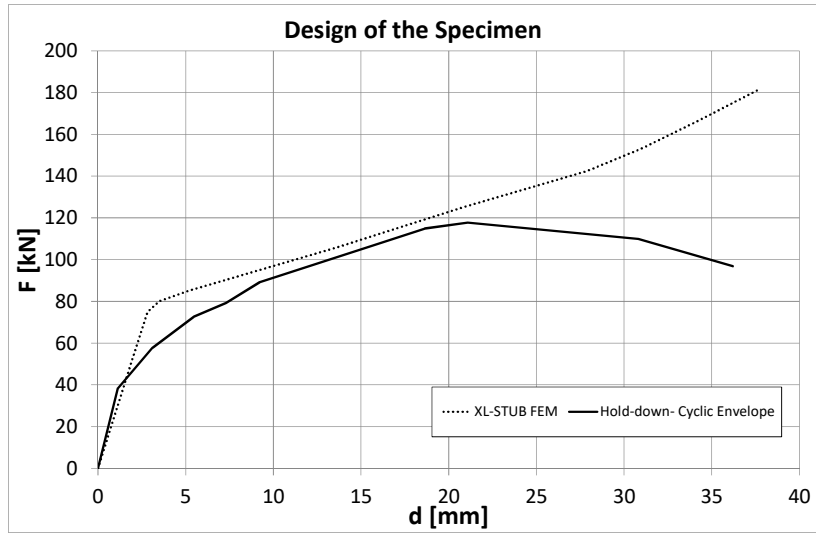
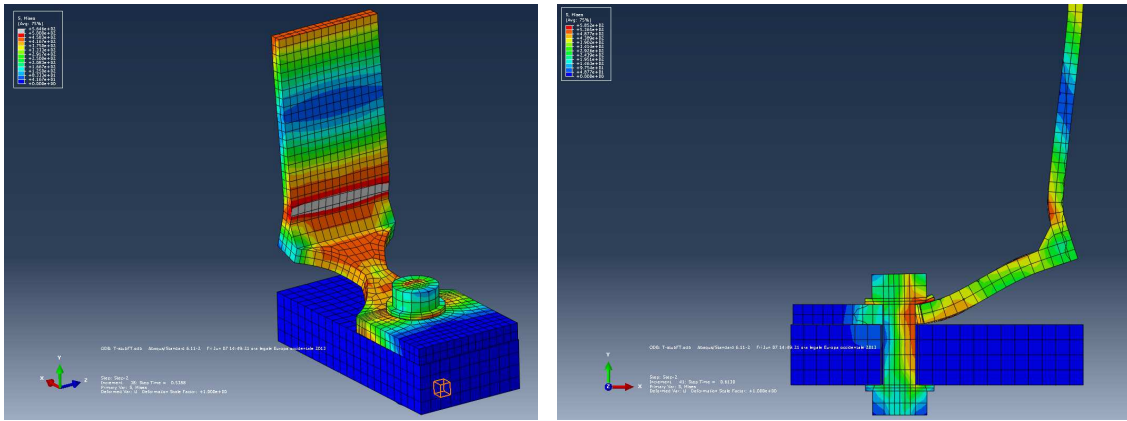
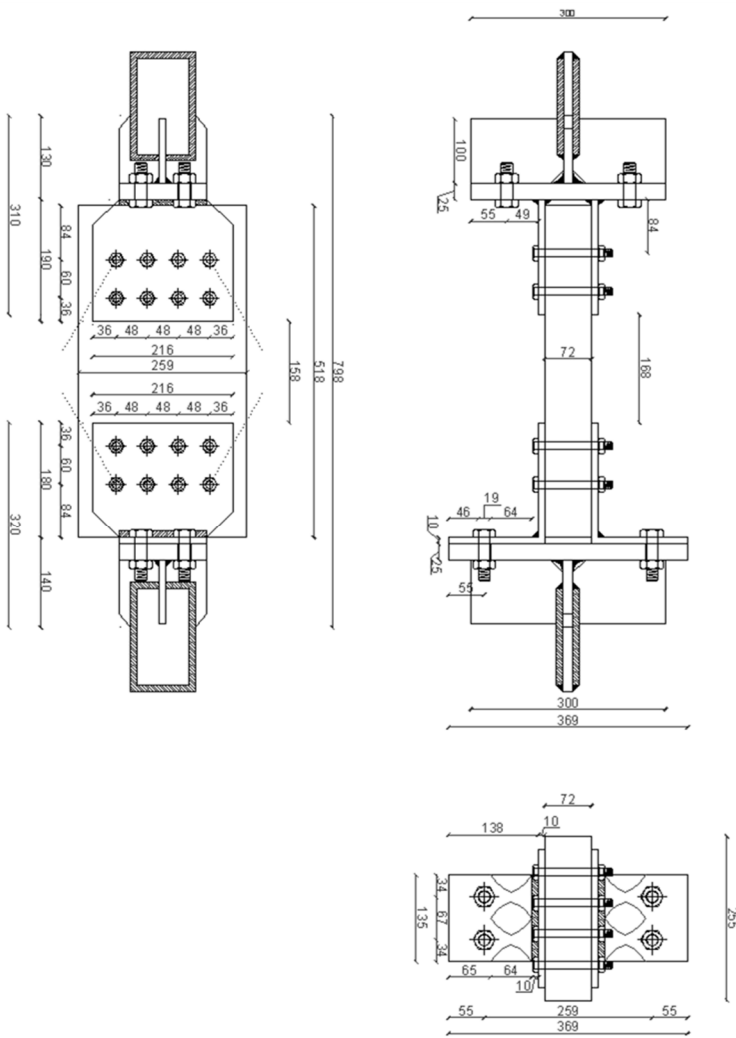


Figure 8. Comparison between hold-down and the ABAQUS simulation of the XL-stub



**Figure 9.** Von Mises Stresses in the XL-Stub – perspective view and view cut



**Figure 10.** Experimental set-up and test arrangement

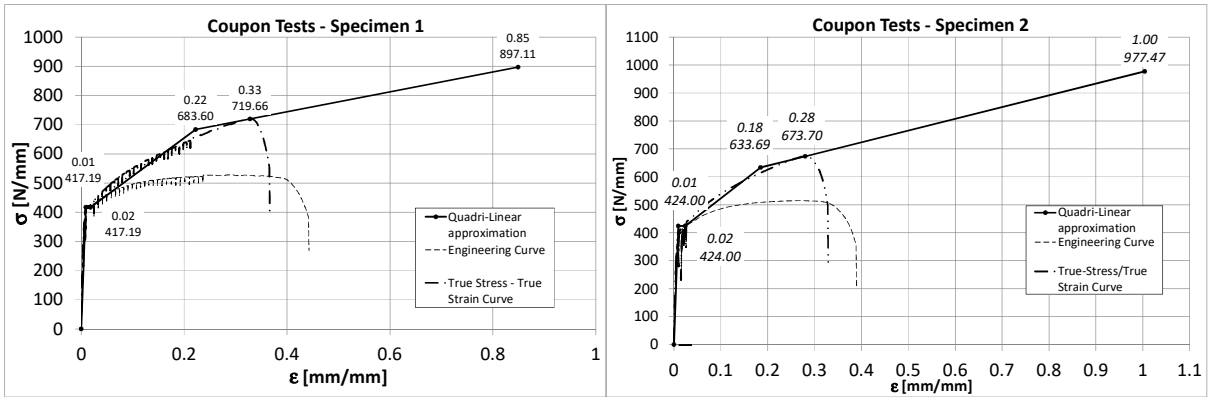
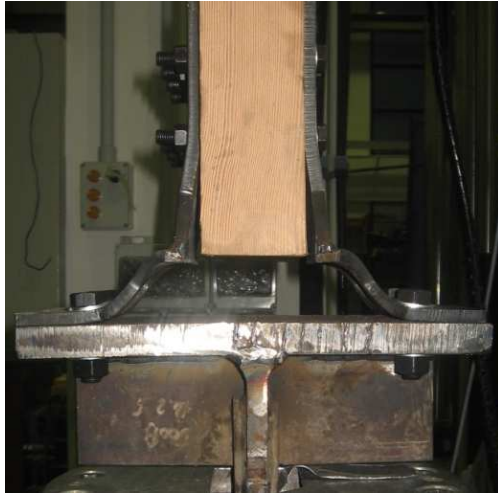
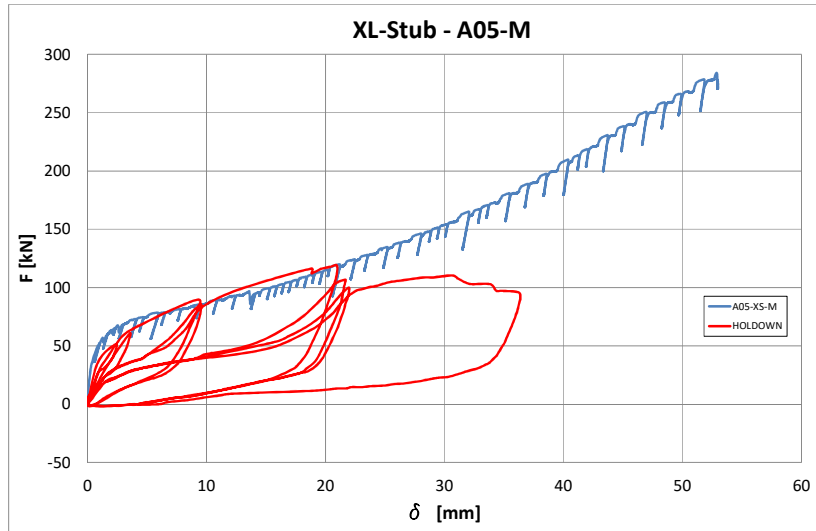


Figure 11. Coupon tensile tests



**Figure 12.** Monotonic test



**Figure 13.** Monotonic force-displacement curve



(a) Test A01-C15



(b) Test A02-C25

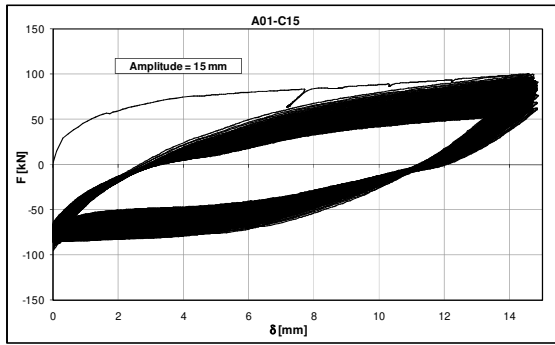


(c) Test A03-C30

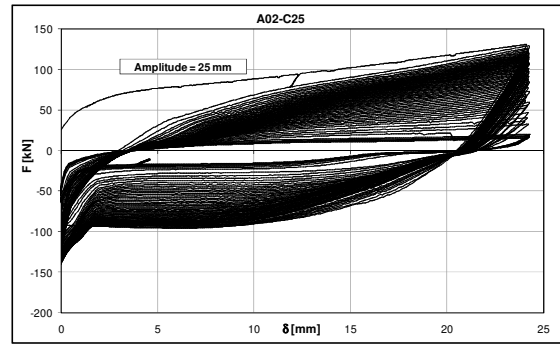
**Figure 14.** Failure modes exhibited by the tested specimens



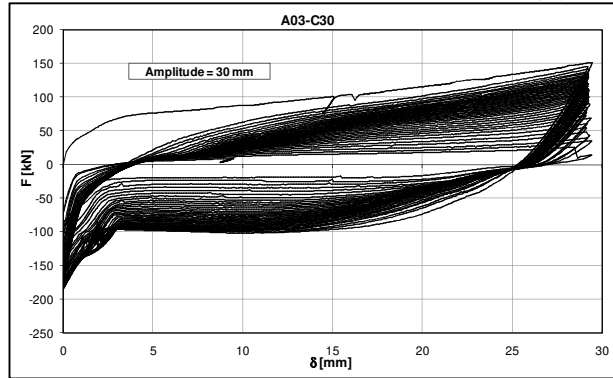
**Figure 15.** Shots took with thermal camera in the first six cycles of loading



(a) Test A01-C15



(b) Test A02-C25



(c) Test A03-C30

**Figure 16.** Force-displacement response of the cyclic tests

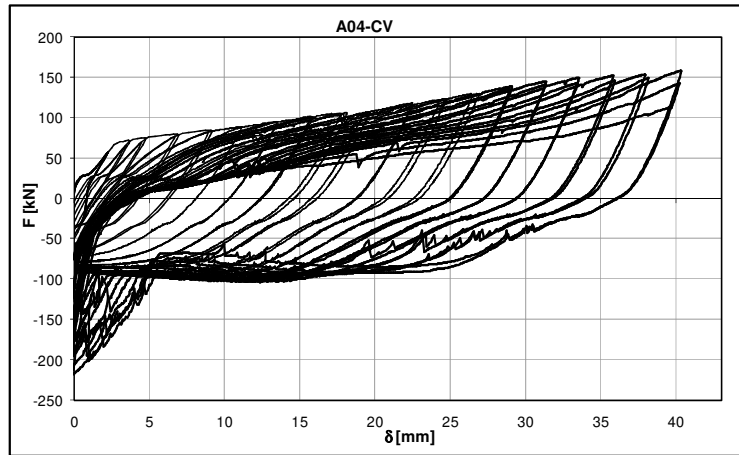
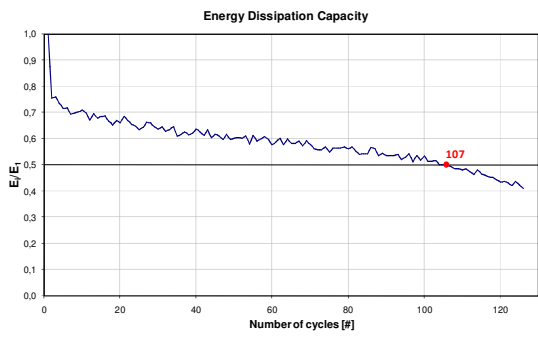


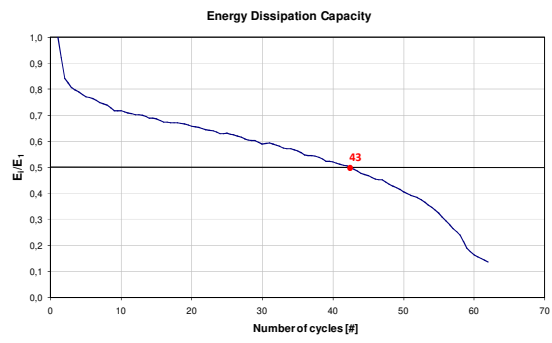
**Figure 17.** Experimental hysteretic response of the XL-stub



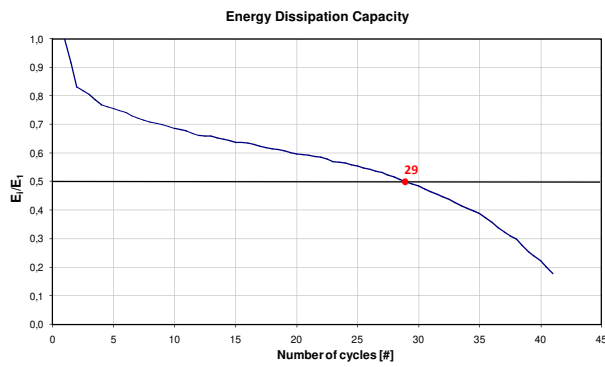
**Figure 18.** Failure of the XL-stub after the variable amplitude cycles test



(a) *Test A01-C15*



(b) *Test A02-C25*



(c) *Test A03-C30*

**Figure 19.** Individuation of the number of cycles at collapse

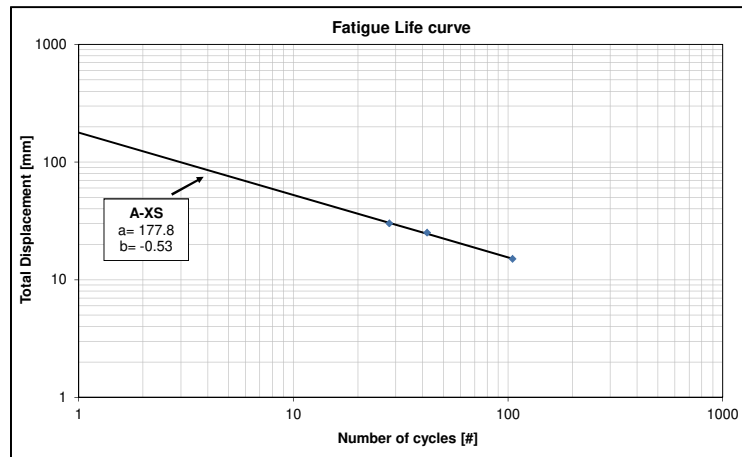


**Figure 20.** Fatigue life curve of the XL-stub

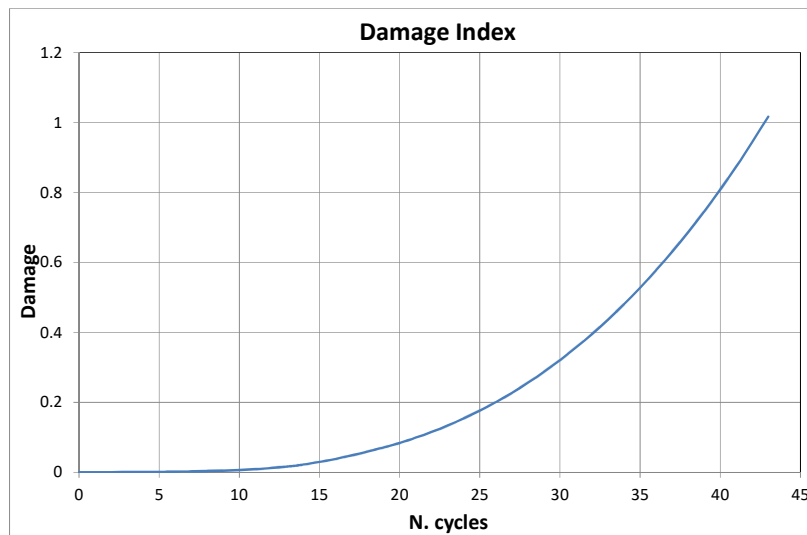


**Figure 21.** Damage index for test A04-CV

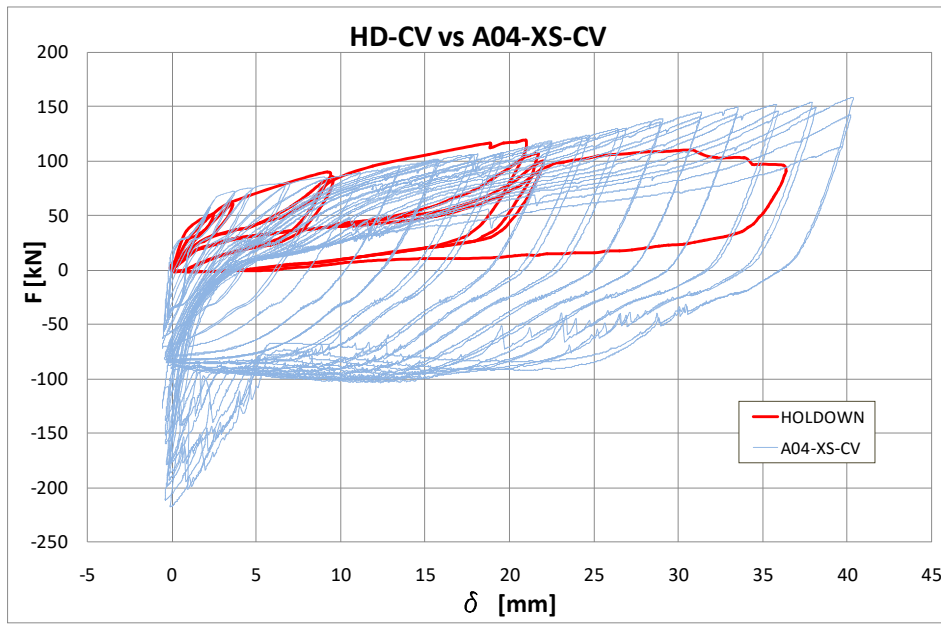
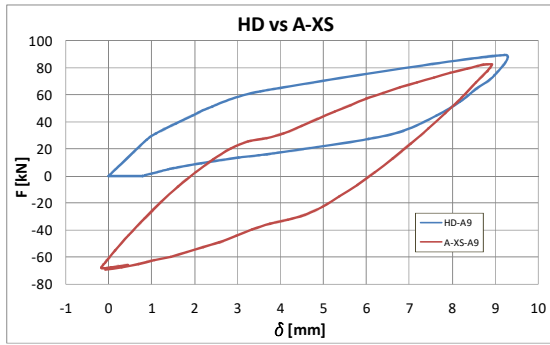
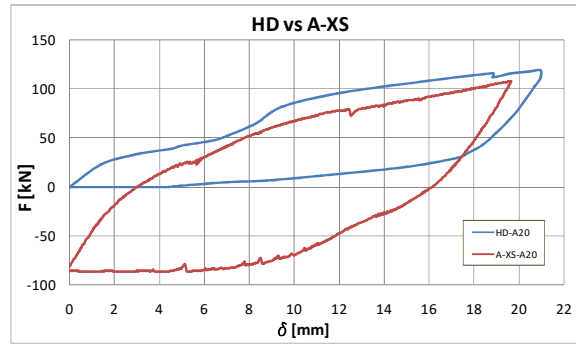


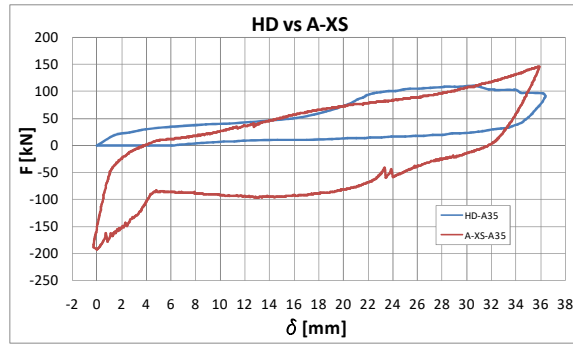
Figure 22. XL-stub vs hold-down



(a) Amplitude 9 mm.



(b) Amplitude 20 mm.



(a) Amplitude 35 mm

Figure 23. Comparison of single cycles at different values of the amplitude

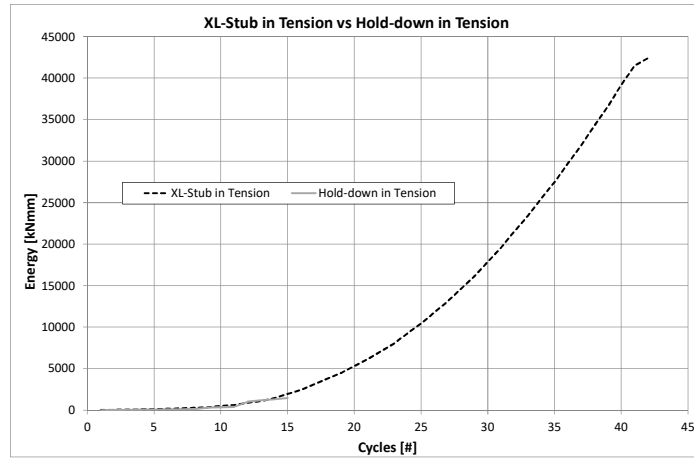


**Figure 24.** Energetic comparison hold-down vs. XL-Stub

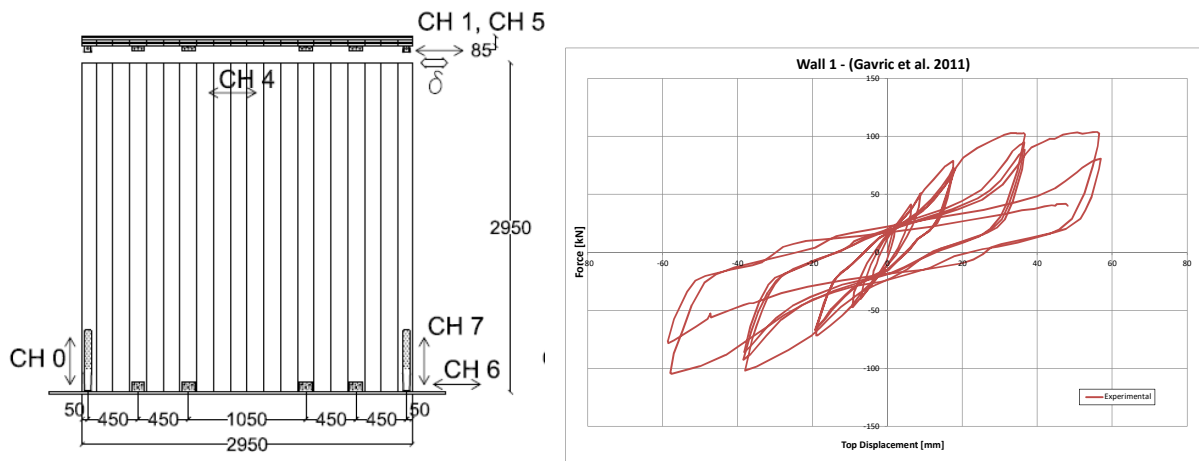
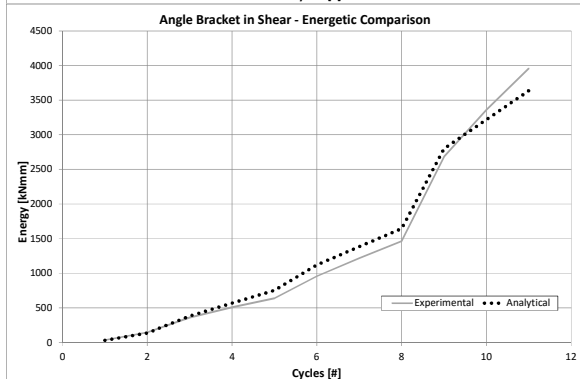
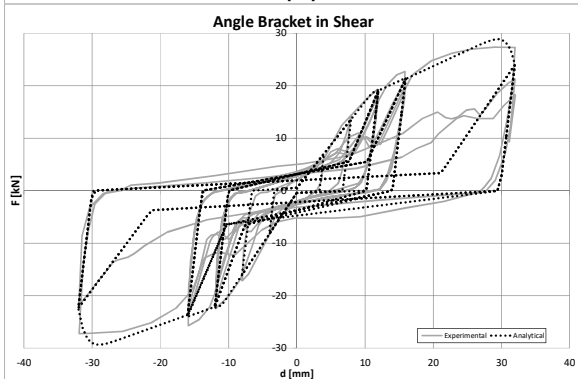
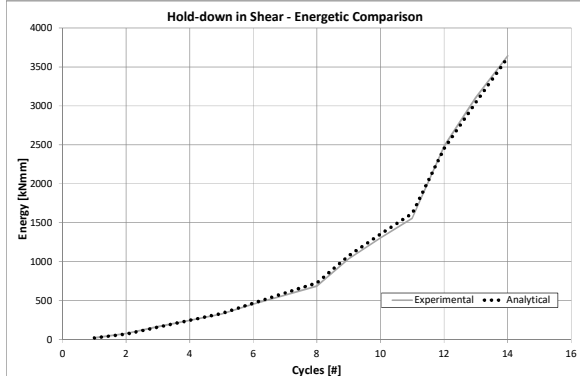
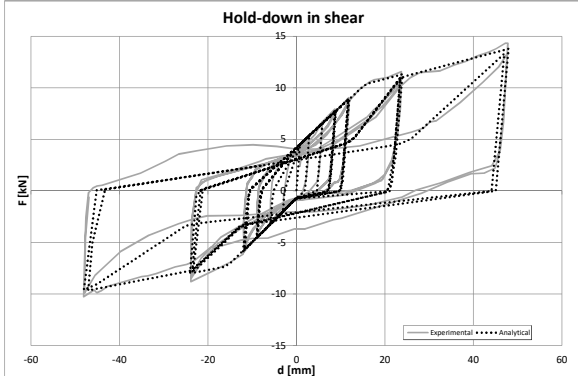
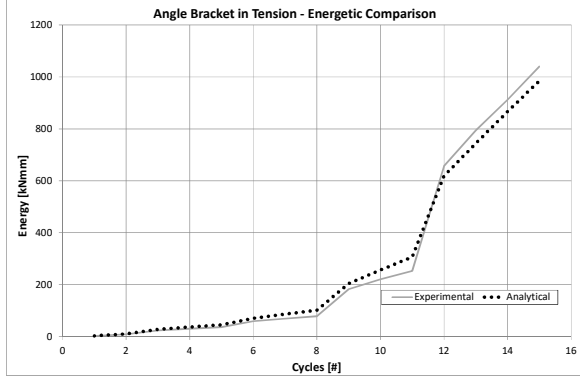
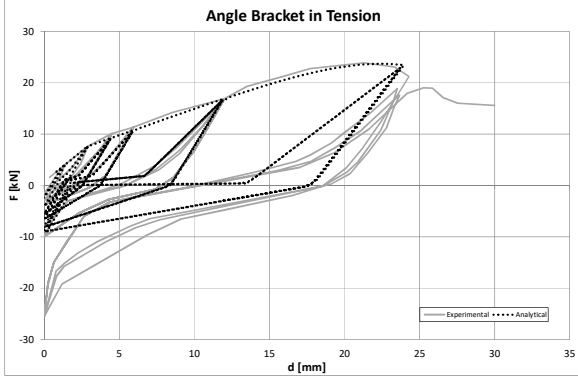
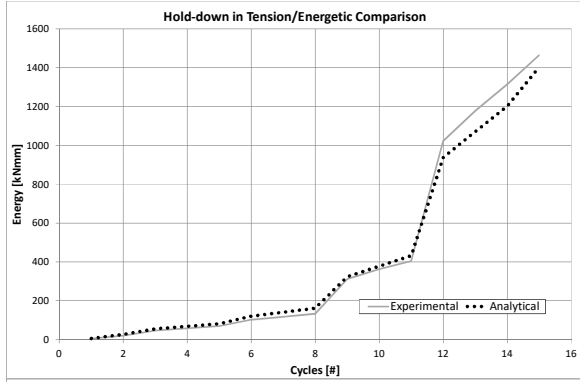


Figure 25. Wall 1 tested by Gavric et al., 2011



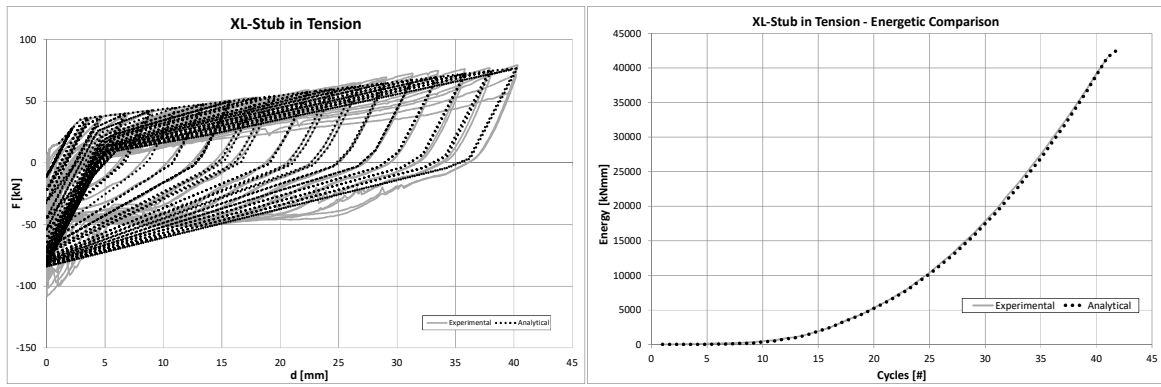


Figure 26. Calibration of the connectors' hysteretic laws

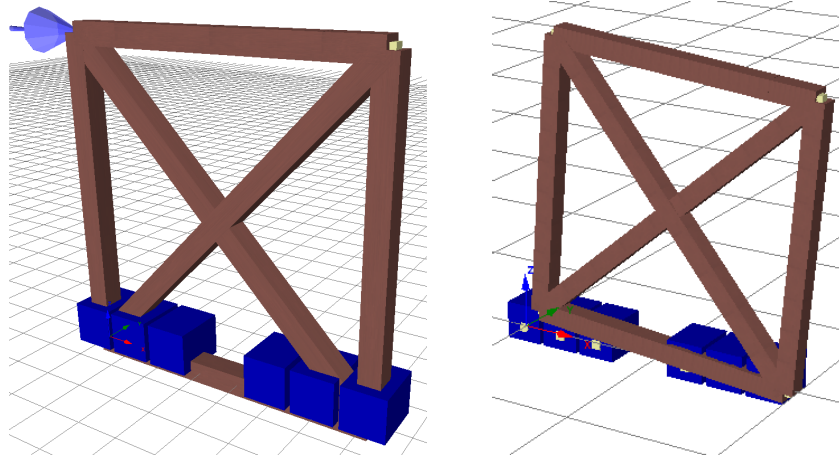
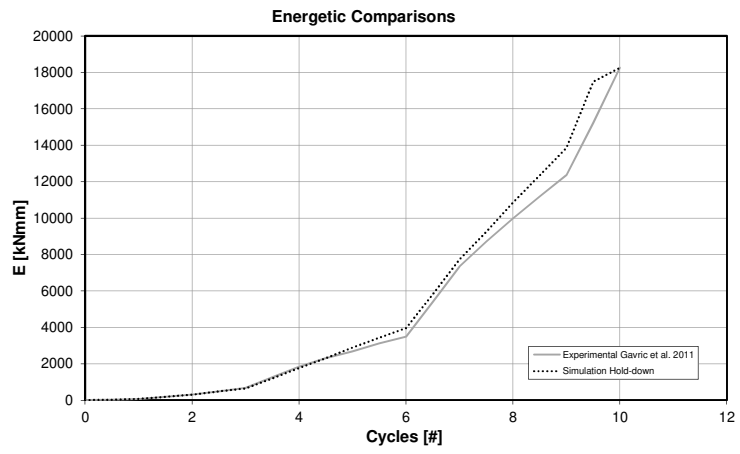
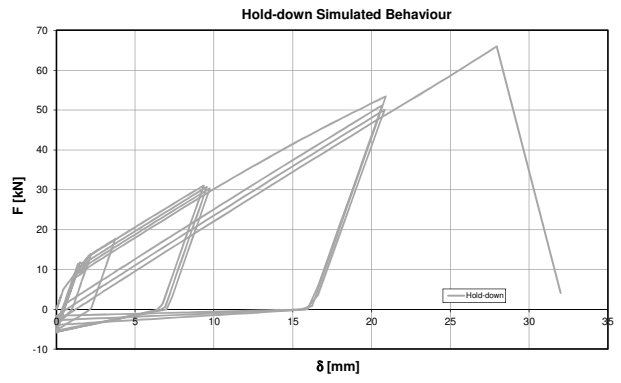
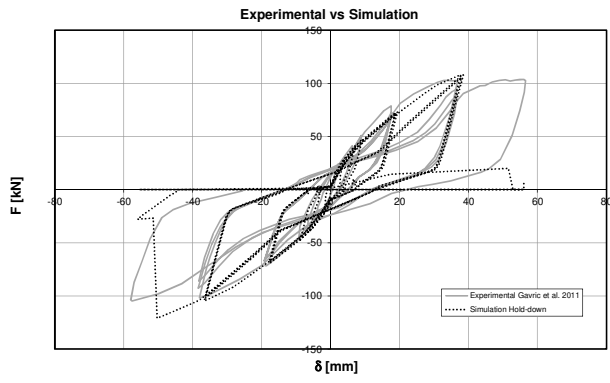
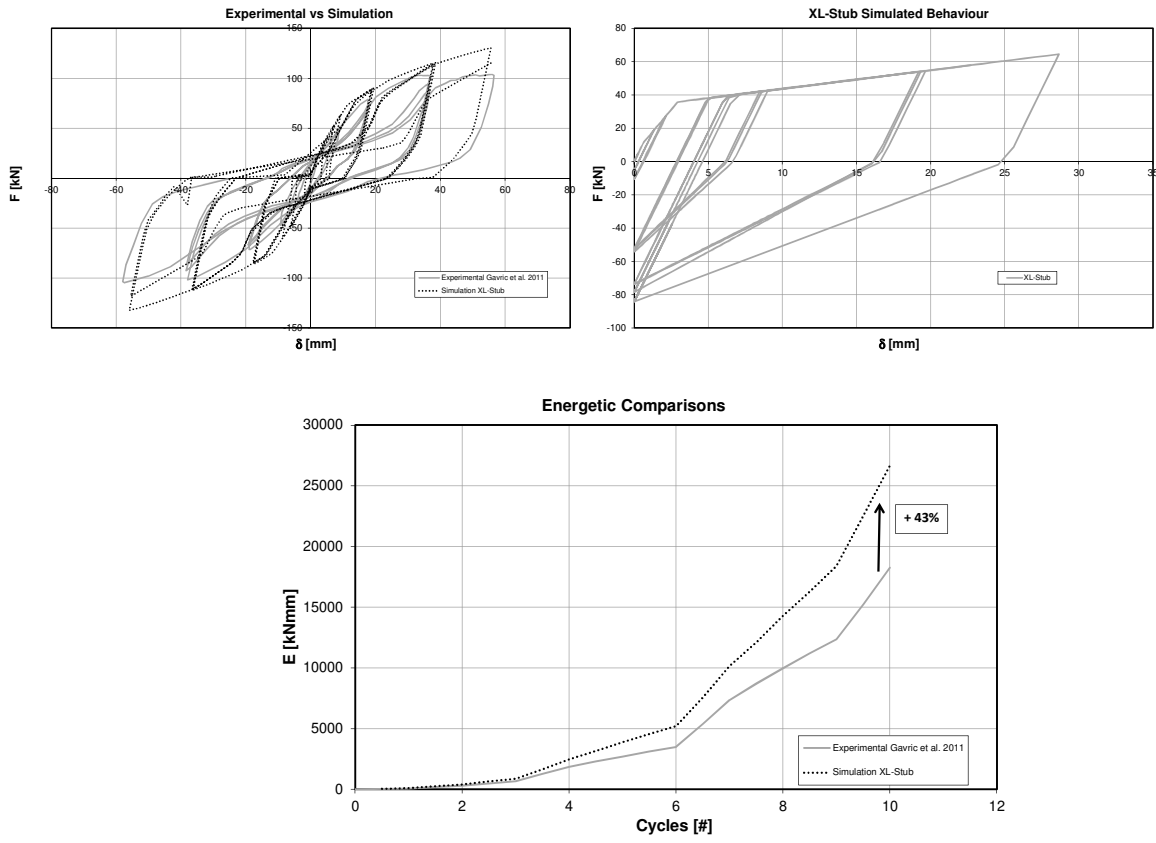


Figure 27. Model in Seismostruct



**Figure 28.** Finite element model vs. experimental



**Figure 29.** Finite element model with XL-stub vs. experimental

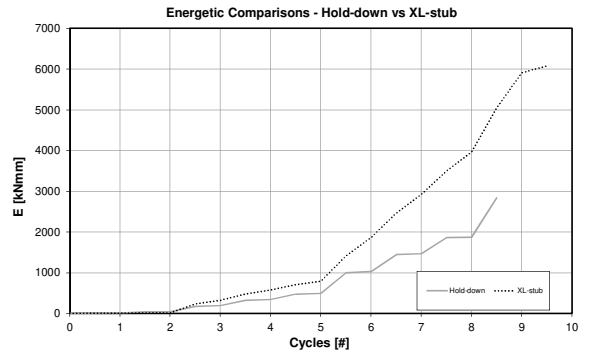
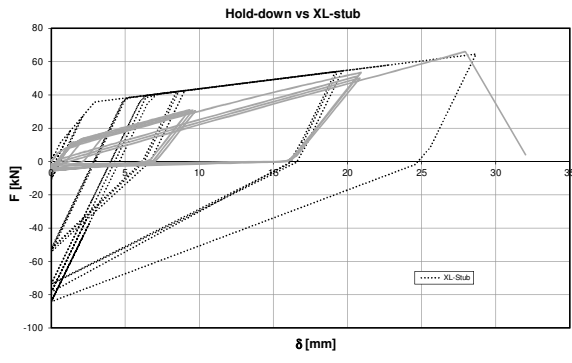


**Figure 30. Hold-down vs. XL-stub**

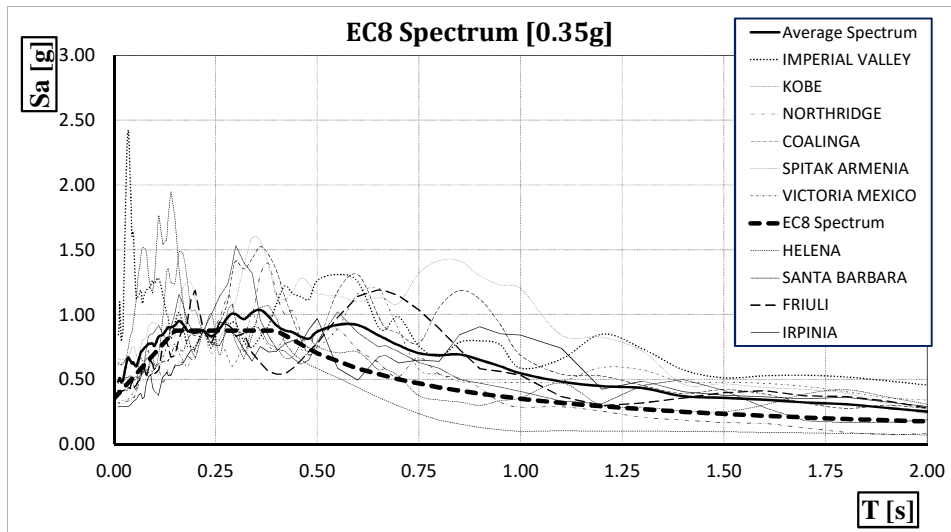
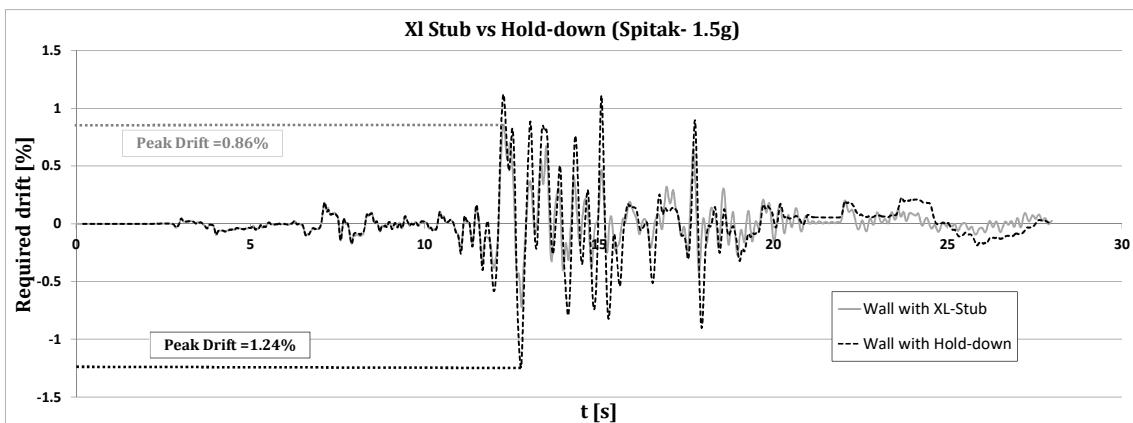
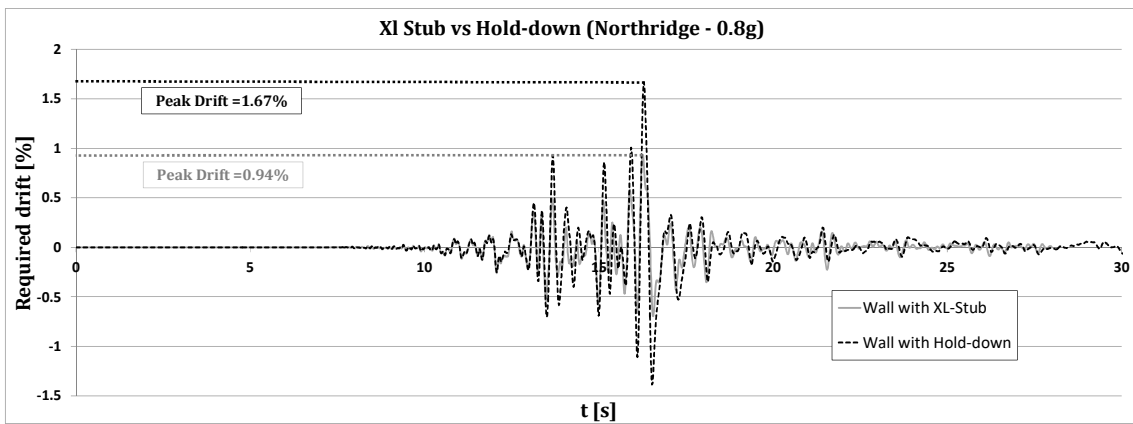
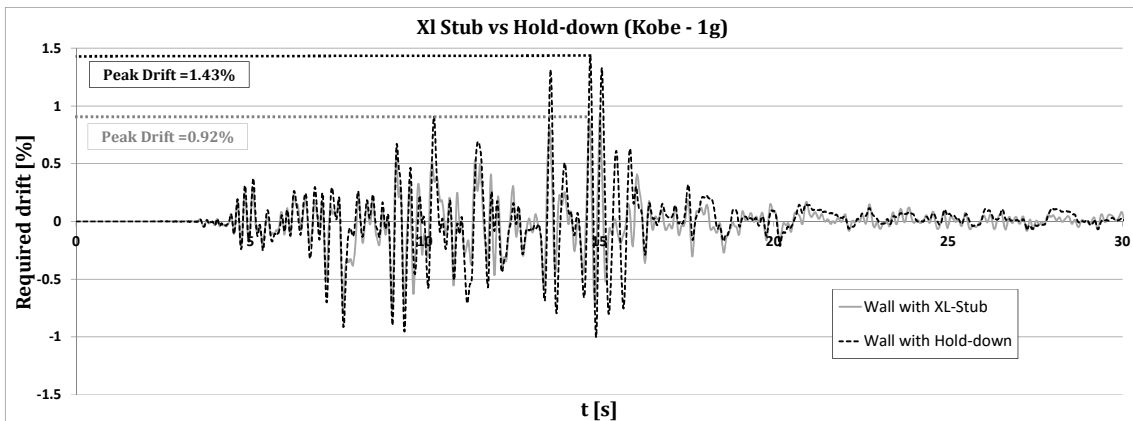
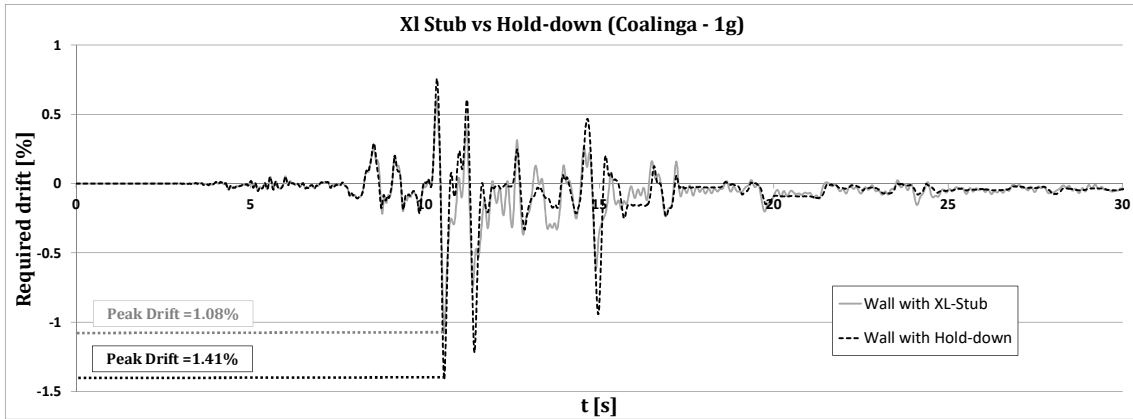


Figure 31. Reference Spectrum and considered earthquakes



**Figure 32. Hold-down vs. XL-stub (Time-History Analysis)**

**Table 1.** Definition of dissipative mechanisms of a steel angle

<b>Failure Mechanism</b>	<b>Dissipative</b>	<b>Non-Dissipative</b>
<b>Splitting failure of wood</b>		X
<b>Failure of the stem</b>	X	
<b>Bearing failure of the nails</b>	X	
<b>Anchor bolt failure</b>		X
<b>Flange plate failure</b>	X	

**Table 2 – Geometrical Properties of the Specimens**

<b>Specimen</b>	<b><math>t_f</math> [mm]</b>	<b>B [mm]</b>	<b>s [mm]</b>	<b>m [mm]</b>	<b>n [mm]</b>	<b><math>d_b</math> [mm]</b>
<b>A01-C15</b>	10	67.5	15	63.9	64.5	18
<b>A02-C25</b>	10	67.5	15	63.9	64.5	18
<b>A03-C30</b>	10	67.5	15	63.9	64.5	18
<b>A04-CV</b>	10	67.5	15	63.9	64.5	18
<b>A05-M</b>	10	67.5	15	63.9	64.5	18

where:  $t_f$  is the flange thickness of the T-stub,  $d_b$  is the bolt diameter and the meaning of the other parameters is illustrated in Fig.5.

**Table 3 – Materials Mechanical Properties**

<b>Specimen</b>	<b><math>f_y</math> [MPa]</b>	<b><math>f_m</math> [MPa]</b>	<b><math>f_u</math> [MPa]</b>	<b><math>\epsilon_y</math> [%]</b>	<b><math>\epsilon_h</math> [%]</b>	<b><math>\epsilon_m</math> [%]</b>	<b><math>\epsilon_u</math> [%]</b>
<b>Coupon 1</b>	417.19	683.6	897.11	0.1	22	33	85
<b>Coupon 2</b>	424	633.69	977.47	0.1	18	28	100

**Table 4.** Loading history under variable amplitudes

$v$ [mm/s]	Step	n° cycles	$\delta$ [mm]	$v$ [mm/s]	Step	n° cycles	$\delta$ [mm]
1	1	5	2.3	8	12	2	25.4
2	2	2	3.5		13	2	27.7
	3	2	4.6		14	2	30.0
	4	2	6.9	15	2	32.3	
	5	2	9.2	16	2	34.6	
4	6	2	11.5	9	17	2	36.9
	7	2	13.8		18	2	39.2
	8	2	16.2		19	2	41.5
6	9	2	18.5		20	2	43.8
	10	2	20.8				
	11	2	23.1				

**Table 5.** Energy dissipation improvement

<b>Displacement Amplitude</b>	<b>Energy Dissipated Hold-Down [kNmm]</b>	<b>Energy Dissipated XL-Stub [kNmm]</b>	<b>Difference [%]</b>
<b>9 mm</b>	338.4	462.7	+36.7 %
<b>20 mm</b>	1202.3	1879.6	+56.3%
<b>35 mm</b>	1908.7	4354.9	+128 %

**Table 6.** Parameters for the cyclic laws of the connectors

Model Parameters	XL-Stub		Angle Bracket		Hold-Down	
		Tension	Tension	Shear	Shear	Tension
<b>EI - Initial Flexural Rigidity</b>	kN/mm	18.33	4.93	11.05	5.69	11.41
<b>PCP - Cracking Force (positive)</b>	kN	11.29	1.38	0.59	4.51	5.054
<b>PYP - Yield Force (positive)</b>	kN	35.73	7.6	18.68	10.61	13.637
<b>UYP - Yield Displacement (positive)</b>	mm	2.94	2.89	11	15.66	2.088
<b>UUP - Ultimate Displacement (positive)</b>	mm	53	25	33	50	28
<b>3P - Post Yield Flexural Stiffness (positive) as Ratio of EI</b>	-	0.061	0.21	0.049	0.02067	0.2
<b>PCN - Cracking Force (negative)</b>	kN	-150	-40	-0.43	-0.74	-45
<b>PYN - Yield Force (negative)</b>	kN	-150.001	-40.001	-21.91	-7.53	-45.001
<b>UYN - Yield Displacement (negative)</b>	mm	-8.1833	-8.1136	-11	-15.66	-3.9439
<b>UUN - Ultimate Displacement (negative)</b>	mm	-100	-100	-33	-50	-100
<b>3N - Post Yield Flexural Stiffness (negative) as Ratio of EI</b>	-	0.999	0.999	0.034	0.0148	0.999
<b>HC - Stiffness Degrading Parameter</b>	-	2000	200	2000	200	2000
<b>HBD - Ductility-based Strength Decay Parameter</b>	-	0.01	0.2	0.05	0.001	0.5
<b>HBE - Hysteretic Energy-based Strength Decay Parameter</b>	-	0.01	0.2	0.03	0.05	0.5
<b>HS - Slip Parameter</b>	-	0.65	0.25	0.3	0.47	0.15

**Table 7.** Energy dissipated by the model vs. experimental

<b>n°cycles</b>	<b>E<sub>diss,exp</sub> [kNmm]</b>	<b>Ediss,mod [kNmm]</b>	<b>Ratio</b>	<b>n°cycles</b>	<b>E<sub>diss,exp</sub> [kNmm]</b>	<b>Ediss,mod [kNmm]</b>	<b>Ratio</b>
0	0	0.0		5.5	3115	3426.0	1.10
0.5	15	20.7	1.35	6	3481	3947.5	1.13
1	59	68.1	1.15	6.5	5381	5809.0	1.08
1.5	186	181.7	0.98	7	7336	7715.5	1.05
2	299	291.9	0.98	7.5	8705	9238.1	1.06
2.5	475	477.2	1.01	8	9969	10849.2	1.09
3	664	639.9	0.96	8.5	11183	12341.9	1.10
3.5	1252	1188.7	0.95	9	12344	13845.2	1.12
4	1833	1760.8	0.96	9.5	15223	17478.6	1.15
4.5	2300	2304.1	1.00	10	18256	18250.5	1.00
5	2677	2881.3	1.08				
<b>Average</b>							1.06
<b>Standard Deviation</b>							0.094